POLITECNICO DI TORINO

Master's Degree Course in Biomedical Engineering

Master's Thesis

Endovascular coiling treatment of cerebral aneurysm: a hemodynamic analysis and a cost-efficacy analysis

Supervisors
Prof. Umberto Lucia
Dr. Massimiliano Povero
Co-supervisor
Giulia Grisolia

Candidate
Miriam Leone 263499

March 2021

"Throw your heart over the obstacle."

Acknowledgments

I thank the enormous human network of connections created during these years of university, where in every knot there is a face with its own history and an indelible memory in my heart. A special thanks go to the most important junction knots of the net, which are those central and solid that will last a long time, a bit like a sailor's knot. These knots have the face of mum, dad, my sister Rosa, my best friend Michele and the group of friends of a lifetime.
Two special thanks:
to my supervisor Umberto Lucia for guiding me and for the trust given in these months of work,
to Massimiliano Povero (AdRes Health Economics and Outcomes Research s.r.l. , Turin, Italy) for the support and valuable advice shown to me during my thesis internship.

Contents

Abstract

The cerebral aneurysm is a localized dilatation of an arterial wall and its rupture is a devastating event associated with high rates of morbidity and mortality. Therefore, it becomes of crucial importance to investigate the alteration of mechanical properties and blood flow in the cerebral artery associated with the formation and growth of the aneurysm.
Endovascular coiling treatment, due to its minimally invasive nature, is being used increasingly as an alternative to the more invasive strategies for brain aneurysm. Like any surgical procedure, intra-procedural complications may occur with an increased risk of morbidity and mortality. Doctors could use Fluid-Structure Interaction (FSI) simulation, a powerful tool for studying and quantifying hemodynamic outcomes in an anatomically ideal model of a brain aneurysm and the effects of endovascular coiling treatment. FSI performed before surgery helps predict the clinical outcomes of a specific coiling treatment and further complications, and thus adverse outcomes could be avoided.
In this work, the first goal is to numerically study the interaction between the blood flow and the middle cerebral artery (MCA) aneurysm wall using the FSI method on the COMSOL Multiphysics platform. Two cases are chosen: an untreated thin wall and a treated MCA aneurysm. For each case, two subcases are examined: Newtonian and non-Newtonian blood model and the effect on the hemodynamic parameters of the blood flow such as velocity pattern, displacement, Von Mises stress and wall shear stress.
Considering the clinical results in their totality, so including in addition to the health outcomes also the clinical costs, it is equally important to conduct a cost-effectiveness analysis in order to help the decision maker, that could be a doctor, about the best clinical path to follow. This arises from the great variety of cerebral coils that can be used in endovascular coiling treatment, and each of these types produces different outcomes.
Work in progress aims to investigate what the most cost-effective cerebral coils choice might be. In the current study, the incremental cost-utility of two macro families of cerebral coils, Spectra Bare Platinum coils versus the other coils, are assessed, including procedural costs, long-term outcomes, and aneurysm recurrence. The Spectra Bare Platinum coils are chosen for their potential cost savings with the decreased stent request due to their particular structure. A decision-analytical study is performed with Markov modeling methods to simulate patients with a cerebral aneurysm undergoing S-BP coiling or alternative coiling. Input parameters are collected from literature review, and a one-way deterministic analysis (DSA) and probabilistic sensitivity analysis (PSA) are performed to investigate the impact of the single parameters variation and uncertainties of all input parameters on the results, respectively.
From the hemodynamic analysis it was found that blood flow forms a vortex in the aneurysm sac due to the slowing of the flow itself. Newtonian model doesn't differ much to the non-Newtonian one, but it causes the overestimation of velocity blood. Therefore, it was found that the blood viscosity has no significant effect on Von Mises stress magnitude and distribution, but there is a strong relation with wall shear stress, since an increase in viscosity causes an overestimation of the wall shear stress peak value. This wall shear stress variation can possibly alter the mechanical properties of the aneurysmal wall inaccurately estimating its rupture risk. It was shown that by treating the aneurysm, the vortex of blood flow and the low wall shear stress area in the aneurysm sac are removed, which suggests the endovascular coiling method as an appropriate treatment of the cerebral aneurysm.
From the cost-utility analysis endovascular treatment using Spectra BP coils was the more cost-effective compared with alternative coiling in the base case. This result was also confirmed in the DSA and PSA. So, this study indicates that S-BP coiling is the dominant strategy with a lower aneurysm retreatment rate and an analogous longer lifetime survival, as well as better health outcomes.

Chapter 1

Intracranial Aneurysm

1.1 Definition

An intracranial aneurysm is an abnormal confined dilatation of a cerebral artery part due to weakening of the vessel's wall [1].
The most frequent sites (*figure 1.1*) are at the level of the intracranial carotid artery, the posterior or anterior cerebral arteries, or the communicating branches of the Willis circle, mostly at arterial bifurcations that are the greater mechanical stress areas [2].

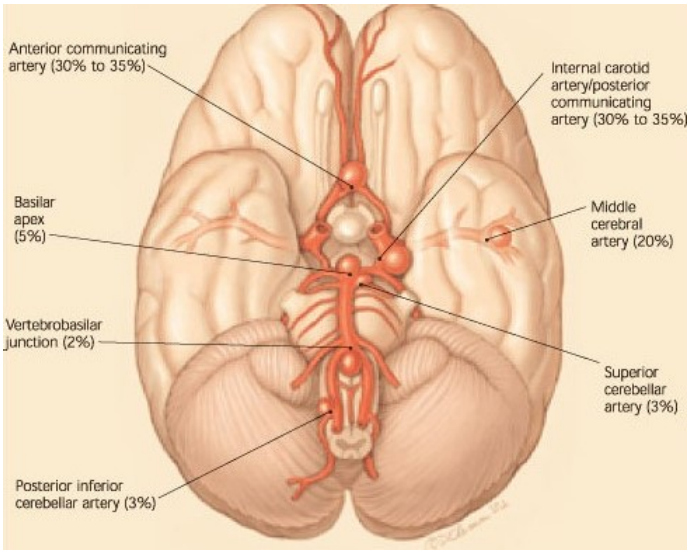

Figure 1.1: Common locations of intracranial aneurysms, with approximate incidences [3].

1.1.1 Classification

The classification of brain aneurysm is based on shape, size and site.
In reference to the diameter size, the aneurysms are distinguished as follows:[1]

- *Small aneurysms* than less of 11 mm;
- *Large aneurysms* from 11 to 25 mm;
- *Giant aneurysms* from 25 to 50 mm;
- *Super-giant aneurysms* over 50 mm.

In reference to the shape, the aneurysms are distinguished as follows:[1]

- *Saccular aneurysm* characterized by the dome, a rounded area and a neck connecting the aneurysm to its parent artery. They are the most common form of cerebral aneurysm;
- *Fusiform aneurysm* appears as a bulges on the all sides of a blood vessel;
- *Charcot–Bouchard aneurysm* is a microaneurysm and typically occurs in small blood vessels of the basal ganglia, due to the chronic hypertension;
- *Dissecting aneurysm* in which an artery wall rips longitudinally;
- *Mycotic aneurysm* due to a bacterial infection of the cerebral arteries that weakens the vessel walls resulting in the formation of a bulge;
- *Ruptured aneurysm*, also called *subarachnoid haemorrhage* (SAH) occurs when aneurysm ruptures followed by bleeding into the space around the brain.

The main types of intracranical aneurysm are illustrated in the *figure 1.2*.

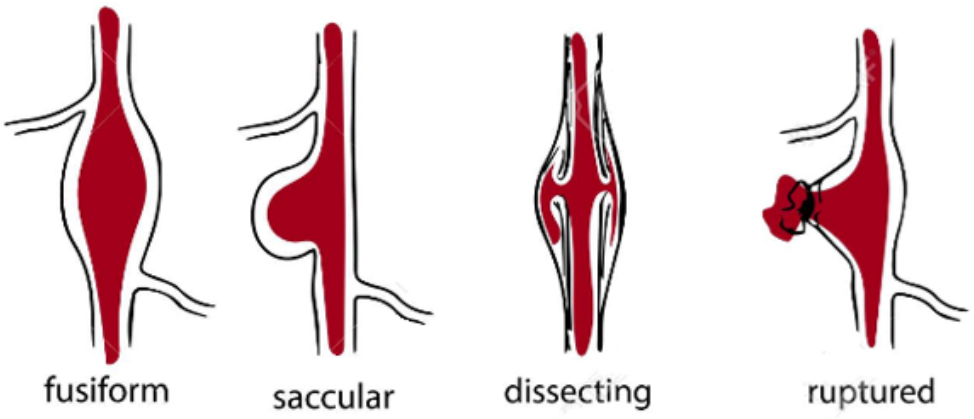

Figure 1.2: Types of intracranial aneurysm [45].

1.1.2 Anatomy

The cerebral arterial circle also known as Willis' circle is a circulatory anastomosis that ensures the blood supply to the whole brain and surrounding structures [5] (see *figure 1.3*).
It is composed by a set of the following arteries:[6]

- Anterior cerebral artery (left and right);
- Anterior communicating artery;
- Internal carotid artery (left and right);
- Posterior cerebral artery (left and right);
- Posterior communicating artery.

The heptagon structure of Willis's circle creates redundancy in the cerebral circulation. In presence of stenosed arteries, blood flows from the other blood vessels preserving the cerebral perfusion to avoid ischemia [7].

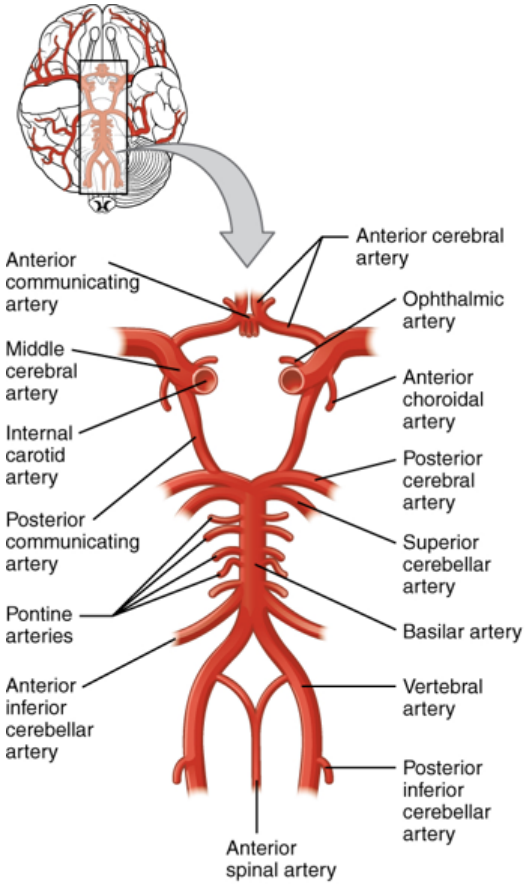

Figure 1.3: Circle of Willis. The blood supply to the brain enters through the internal carotid arteries and the vertebral arteries, eventually giving rise to the circle of Willis [4].

1.2 Symptoms, complications and risk factors

An unruptured aneurysms may be:[1]

- asymptomatic and casually discovered during clinical findings done for other causes;
- symptomatic because they compress adjacent structures. Ocular palsies, eye pain, squint may be due to pressure on cranial nerves. Vision deficits may be due to pressure on the optic chiasm.

After an aneurysm has ruptured it may cause symptoms such as:[1]

- sudden and severe headache called a thunderclap headache;
- nausea and vomiting;
- loss of consciousness;
- photosensitivity;
- seizures;
- motor deficits;
- cranial nerve deficits;
- coma and death.

After an aneurysm's rupture, the following complications may arise:[1]

- Rebleeding: an aneurysm that has ruptured is at risk of a second haemorrhage causing further damages to the brain cells;
- Hyponatremia: is an imbalance sodium level in blood due to the SAH and a lowering of sodium levels is followed by a swelling causing permanent brain damage;
- Hydrocephalus: SAH can cause cerebrospinal fluid's circulation which causes pressure inside the brain damaging tissues and/or leading to coma or death;
- Vasospasm: after SAH, blood vessels may narrow and limit blood flow to a portion of the brain causing an ischemic stroke.

The most common factors contributing to the development of intracranial aneurysm are:[1][2]

- hypertension,
- smoking,
- alcoholism,
- obesity,
- cocaine use,
- head trauma and infection,
- hereditary connective tissue disorders (e.g. Ehlers-Danlos syndrome, pseudoxanthoma elasticum, autosomal dominant polycystic kidney syndrome),
- family history of aneurysm.

The aneurysm occurrence is among people aged 30 to 60 years and women are particularly subjected[1].

1.3 Diagnosis

Diagnostic examinations used for a cerebral aneurysm may include:

- *Computed tomography angiography* (CTA): is a combination of X-ray computed tomography (CT) and radiocontrast, in general, iodine-based types, used for viewing better the brain blood vessels and localizing the aneurysm position, as shown in the *figure 1.4* [1].

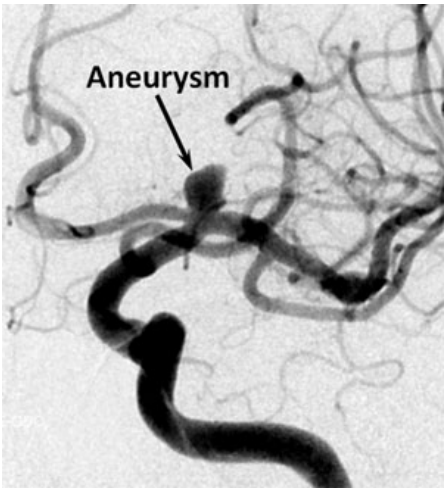

Figure 1.4: Brain Aneurysm, Radiology [8].

- *Digital subtraction angiography* (DSA): is an invasive procedure, adopted when the others are not sufficient. A microcatheter is inserted into the femoral artery and led to the brain blood vessels [1]. The catheter is filled with a contrast dye and X-ray images of the blood vessels are acquired [1].

- *Magnetic resonance imaging* (MRI): is a non-invasive procedure which involves magnetic fields to detect the minimum fluctuations in brain tissues that are useful to locate and diagnose a stroke [1]. If an intravenous contrast dye is injected, the Magnetic resonance angiography (MRA) is practiced, that makes the blood vessels opaque, differentiating them from everything else [1].

1.4 Treatment

Before deciding which is the most appropriate treatment for brain aneurysm, several factors should be taken into account: size, type and location of the aneurysm, the patient's age and health, the presence or absence of symptoms, and the risk factors for aneurysm rupture and risks of treatment [2].
Not all aneurysms require immediate treatment, infact, if an asymptomatic aneurysm's size is < 7 mm located in the anterior circulation rarely rupture and can be monitored with imaging techniques [2].
Treatments aim to the obliteration of the aneurysm avoiding the rupture or stopping the bleeding. There are many surgical procedures which can be grouped into two main categories:

- *Surgical clipping*: First attempts date back to 1937, when American neurosurgeon Dandy sealed an aneurysm's neck of the internal carotid artery with a V-shaped clip [10].
  The clipping is an open surgical procedure which involves an opening on the skull and once the aneurysm has been exposed and isolated from other brain tissues, it is sealed with metal clips, whose form and size depend on the aneurysm characteristics, and that prevent blood flow from entering the aneurysm dome [10].
  The result of this treatment is illustrated in the *figure 1.5*. Some larger giant aneurysms originated from important brain blood vessels cannot be treated with surgical clipping that could cause a decrease in brain perfusion resulting in a stroke and the alternative technique is represented by the cerebral bypass [10]. This surgical procedure involves an anastomosis between two arterial vessels ensuring sufficient blood flow to the brain [10].

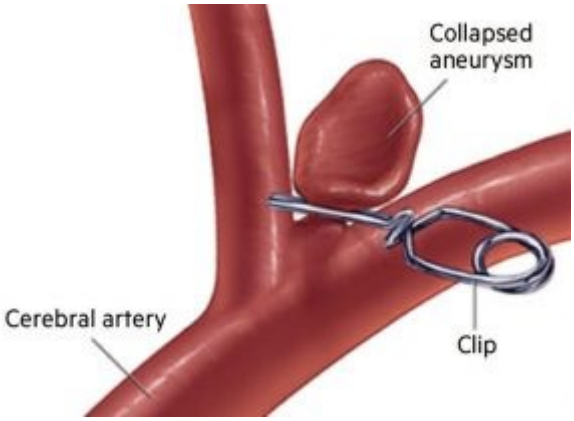

Figure 1.5: Surgical Treatment: Clipping [9].

- *Endovascular coiling*: In 1991 an American neuroradiologist invented the detachable coils (GDCs), a platinum coils, paving the way for a new brain aneurysm treatment, the endovascular coiling or coil embolization [10].
  The most frequently used traditional techniques include *direct coiling*, *balloon-assisted coiling* (BAC), and *stent-assisted coiling* (SAC) [11].

1.4.1 Direct Coiling Techniques

1.4.1.1 Direct Coil Embolization

Direct Coiling is a minimally invasive technique that has the same purpose as surgical clipping, in which a guide catheter is introduced from the femoral artery and led to the brain near the aneurysm, while at the same time an angiography is performed in order to guarantee the correct positioning of the catheter [9]. The tip of the catheter should be placed distal to the orifice of the aneurysm sac (neck) [11].
A tiny platinum coil is advanced through the catheter assuming a straight shape, but when it exits the catheter, it takes a spiral shape, adapting to the shape of the aneurysm [9]. In the presence of larger aneurysms, more coils are used to fill the aneurysm and the blood within it becomes clotted off, preventing rupture [9]. The coil (or coils, as sometimes more than one is needed) prevents blood from flowing into the aneurysm and this leads the blood inside the aneurysm to clot [9]. Once the aneurysm has been wrapped, in angiography no more blood is seen flowing into the dome, indicating that the occlusion was successful [11].
The *figure 1.6* illustrates an overview of the coil embolization procedure.

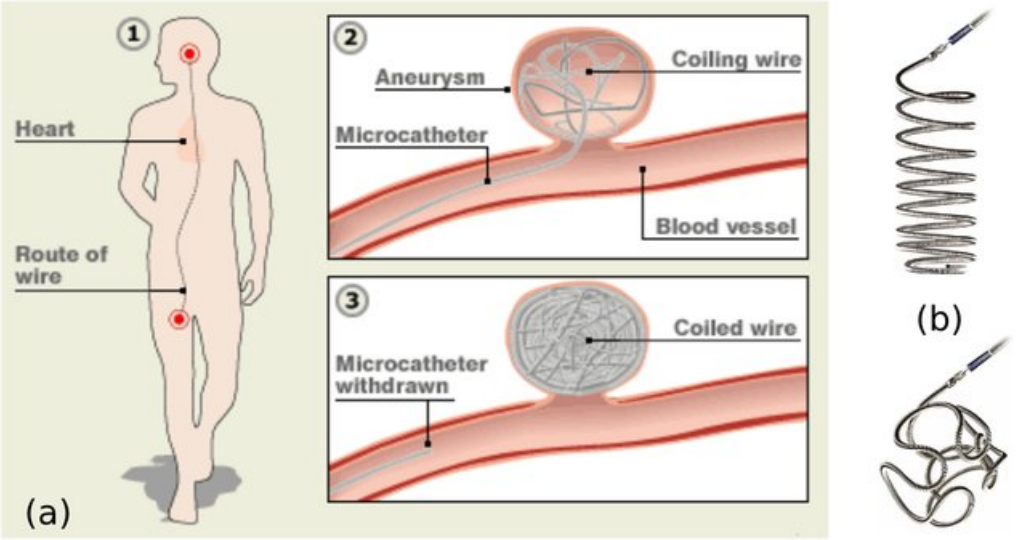

Figure 1.6: (a): Coil embolization procedure: a catheter is inserted into the femoral artery to reach the brain (1) then a micro-catheter is placed near the diseased vessel and coils are inserted in the aneurysm (2) and finally, the micro-catheter is withdrawn and the body starts forming a blood clot around the coils (3); (b): two examples of coils with very different shapes: an helical shape (up) and a complex shape (bottom) [12].

1.4.1.2 Double Microcatheter Technique

The double microcatheter technique is a modified direct coil embolization which involves two micro-catheters, one sited within aneurysmal sac and the other advanced into artery to avoid coil protrusion [11]. From the first catheter a coil is deployed into the aneurysm until to make a loop, then another coil exits from a second catheter, and repeating these steps alternately as long as occlusion is reached, coils brace each other, twisting their loops, and each other prevent their herniation into the artery [11]. The result of the current technique is illustrated in the *figure 1.7*.

Figure 1.7: Illustration of microcatheter placement within the aneurysm followed by the deployment and interleaving of the coils [13].

1.4.2 Ballon-Assisted Coil Embolization

The balloon-assisted coiling (BAC) technique is particularly useful to treat wide-necked aneurysms [14]. In sidewall aneurysms, once advanced guidewire and microcatheter, the balloon catheter is placed around the neck of the aneurysm, as shown in the *figure 1.8*, a balloon is inflated and deflated after the coil is deployed [14]. For the release of further coils, the same procedure is repeated until the aneurysm is completely eliminated.

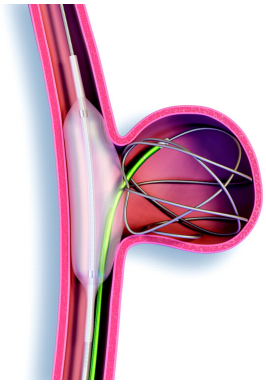

Figure 1.8: Remodeling technique for sidewall aneurysms [14].

A very complex case is the bifurcated aneurysm, because the neck must be protected to avoid coil herniation *(figure 1.9)*[14]. In this situation different strategies can be adopted:[14]

- Inflate a pear-shaped balloon in the bifurcation artery to totally cover the neck *(figure 1.9 A)*;
- Two balloons are placed in front of the aneurysm neck, one on each side of the artery bifurcation *(figure 1.9 B)*;
- A balloon is inflated parallel to the neck of the aneurysm using the Willis circle structure *(figure 1.9 C)*;
- Inflate a double lumen microcatheter balloon in front of the neck with the guidewire inside the neck. The coils are deployed into the aneurysm dome through the second lumen *(figure 1.9 D)*.

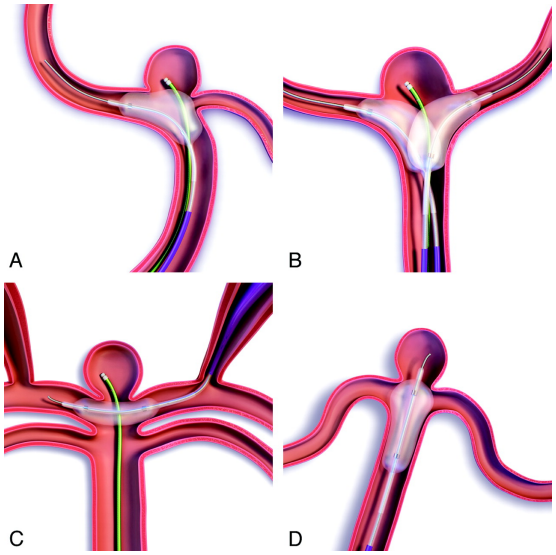

Figure 1.9: Remodeling technique for bifurcation aneurysms: (A) Use of a pear-shaped balloon: (B) Double-balloon technique;(C) Placement of the remodeling balloon parallel to the aneurysm neck by using circle of Willis anastomosis; (D) Use of a double-lumen remodeling technique [14].

1.4.3 Stent-Assisted Coil Embolization Techniques

Some wide-necked or anatomically complicated aneurysms are treated with the stent-assisted coil (SAC) technique [11]. A stent is a tiny, soft, flexible mesh tube made of nitinol, inserted into the parent artery where the aneurysm has formed [9]. This device acts as a mechanical scaffold providing support for coils inside the aneurysm sac avoiding their haerniation into the parent artery, as well as a greater packing [16]. There are several variations of this strategy.

1.4.3.1 Semi-Jailing Technique

First the coil microcatheter is delivered by using a guidewire inside the aneurysm sac and one or two loops are deployed [15]. Later, the stent microcatheter is placed using a guidewire a little above the site of the intracranial aneurysm and partially deployed covering a part of aneurysm neck in order to prevent the coils come out of the sac [15]. The coiling is performed and at only at the end the stent is completely deployed [15]. The basic steps are illustrated in *figure 1.10*.

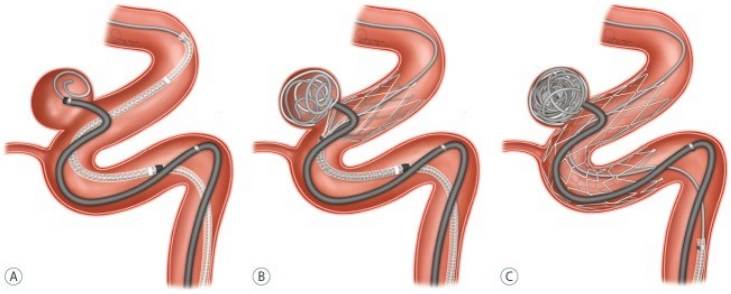

Figure 1.10: Schematic illustration of semi-jailing technique: (A) After some coils delivery, the stent catheter is placed over the aneurysm portion; (B) After the stent is partially deployed, coiling is performed; (C) The stent is fully deployed after achieving the dense coil packing [15].

A variant, *Through-Stent Technique* provides for the release of the stent before that of the coil [11]. The coil microcatheter is advanced inside the aneurysm sac through the interstices of the stent and its

delivery can occur simultaneously with stent placement or in a delayed manner allowing a better stent stability [11].

1.4.3.2 Dual-Crossing Stent Technique, Y-Stent Configuration

The dual-crossing stent technique was introduced to treat wide-necked aneurysms located near a bifurcation brain arteries [11]. The stent delivery microcatheter is placed into one of the branches, while a second microcatheter is advanced using a guidewire close to the aneurysm neck and once the first stent is deployed, its microcatheter is removed [11]. A second stent delivery microcatheter is advanced in the opposite branch through the interstices of the first stent, distributing the second stent and with a smaller cell design to be able to slide into the first without creating problems [11]. In this way, the two stents form a y-configuration. Next, the coiling is performed.
The basic steps are illustrated in *figure 1.11*.

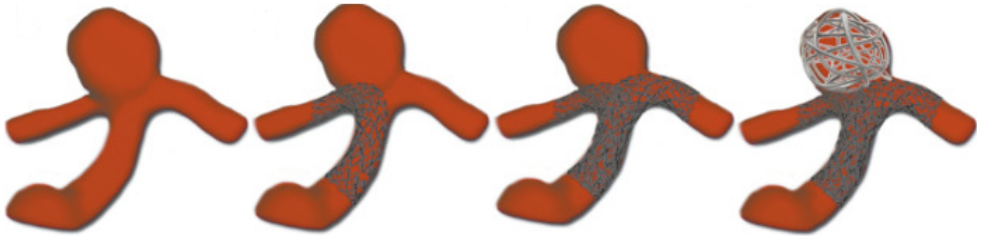

Figure 1.11: The basic steps involved in the Dual-Crossing Stent Technique [11].

1.4.3.3 Shelf Technique

The Shelf technique is used to treat wide neck aneurysms and differs from other stent-assisted methods in the stent delivery phase [11]. A braided stents such as *LVIS Jr.* stent are used that allows to create a shelf around the aneurysm neck avoiding coil migration [17].
The microcatheter is placed over the aneurysm position and stent is deployed covering half of the neck [11]. The stent pusher wire and microcatheter are pushed forward and the stent is deployed in steps of 1 mm as long as it creates a bulge inside the aneurysm neck until to cover 75% [11]. The rest of the stent is delivered with the standard procedure [11]. The coiling may be performed before or after stent placement [11]. The *figure 1.12* shows the final result.

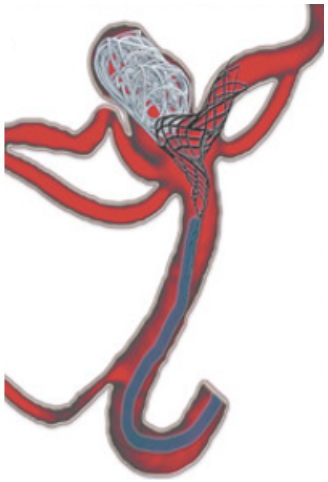

Figure 1.12: Deployment of an LVIS Jr. stent from the left posterior communicating artery into the distal basilar artery via the Shelf technique [11].

1.5 Coiling Results Assessment

The coil packing density (PD) is considered a good indicator of a lasting success of coil embolization [11]. The PD is defined as the ratio between the volume of deployed coils and the volume of an aneurysm as reported in the following formula: [11]

$$\%Packing\ \ density = \frac{V_{coils}}{V_{aneurysm}} \cdot 100 \tag{1.1}$$

where the volume of aneurysm is calculated as follows: [11]

$$V_{coils} = \pi \cdot (radius)^2 \cdot Length_{coil} \tag{1.2}$$

In the literature the importance of this parameter in the treatment of cerebral aneurysm is underlined as it preludes the possibility of a risk of recanalization and the need for retreatment [11].
Several studies show that the incidence of recurrence is significantly lower in presence of packing greater than 25% [11]. The purpose of coiling embolization is to achieve complete obliteration of the aneurysm and the size of the aneurysm has a considerable incidence [11].
The degree of initial occlusion is assessed by Raymond Montreal scale, an angiographic classification structured as follows: [18]

- class I: complete obliteration,
- class II: residual neck,
- class III: residual aneurysm.

Mascitelli et al.[18] proposed the modified Raymond scale (mRS) (*figure 1.13*) subdividing the class III in two subclasses: [18]

- class IIIa: contrast opacification within the coil interstices of a residual aneurysm,
- class IIIb: contrast opacification outside the coil interstices, along the residual aneurysm wall.

Class I and class II show good results, while class III is an indicator of recurrence and/or retreatment [18].

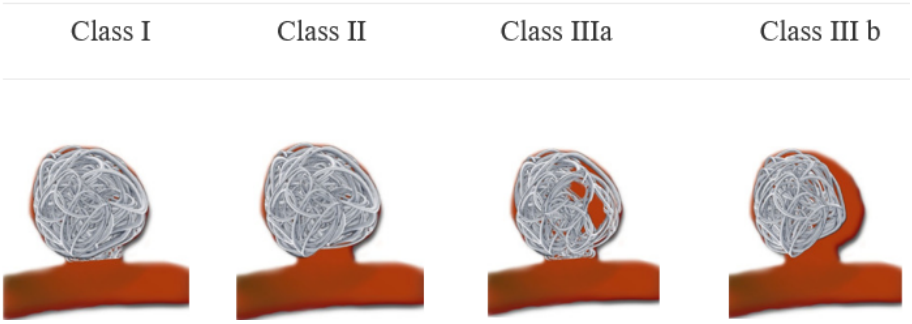

Figure 1.13: Modified Raymond Occlusion Classification [11].

Chapter 2

Families of Coils used in the Endovascular Treatment of Cerebral Aneurysms

A variety of coil types are currently commercially available for clinical use, which differ according to the material used, shape and detachment mechanism into internal aneurysm enviroment.
According to shape, cerebral coils can be divided into *helical coils* and *complex coils* which forms a stable framing across the aneurysm neck *(figure 2.1)*.

Figure 2.1: Helical coil on the left [32]. Complex coil on the right [33].

According to the type of material, there are three categories of coils:[25]

- *Bare platinum coils*,
- *Bioactive coils*,
- stretch-resistant bare platinum coils also known as *Spectra Family coils*.

The first detachable Guglielmi coil (GDC) introduced in 1990 was made of platinum and the detachment from the guide wire took place by electrolysis [34]. In the endovascular treatment of intracranial aneurysms the GDC coils are positively charged with an electric current passage of 1 mA for a total time of about 2 minutes which induces electrothrombosis, the attraction of blood constituents on the surface of the coils, with the hope to trigger thrombosis of the aneurysm sac [23] [24]. The most significant negative outcomes of bare platinum coils were found in the treatment of wide neck aneurysms due to the high rate of recanalization and retreatment [22].
In order to reduce recurrence, a second generation coils were introduced in 2002, known as Bioactive coils, characterized by a polymer coating to achieve a better and faster aneurysm healing, a more stability

coiling and durability of occlusion [22]. Four bioactive coils are commercially available which differ on polymer coating type based: [22]

- PGLA-Coated Coil (Matrix),
- Hydrogel-Coated Coils (HydroCoil),
- PGA-Coated Coils (Cerecyte),
- PGLA fibered Coils (Nexus).

PGLA bioactive agent is a resorbable polymer of 10–90 days, which its inflammatory response occurred when placed into contact with the internal aneurysm environment will induce the acceleration of conversion of thrombus to fibrocellular tissue and thus improve healing and increase packing density as a consequence [22].
The HydroCoil is an expanding Hydrogel-Coated Coil which expansion a three to ninefold increase in size, occurs when deployed into the blood and requires a precise release from the point of view of timing, with a maximum of 5-7 minutes, because the swelling of the hydrogel coating makes recovery through the microcatheter difficult [22]. *Figure 2.2* shows the bioactive coil before and after the expansion. The hydrogel does not degrade easily acting as a substrate that absorbs blood components during the swelling process thus promoting healing and decreasing recanalization rates [22]. Hydrogel coils have a similar safety profile as bare platinum coils, but demonstrated lower rates of aneurysm recurrence and retreatment [22].

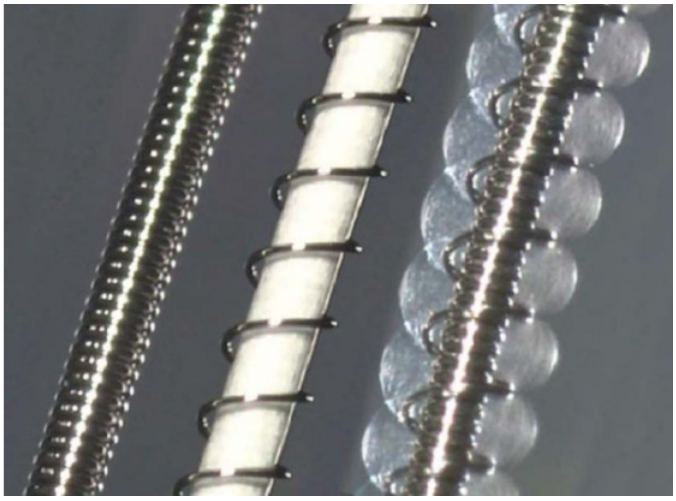

Figure 2.2: Bare platinum coil on the left. Middle, Prehydration image, showing initial profile of the Hybrid hydrogel-platinum coil device where a highly compact hydrogel material is wrapped around a platinum coil and an outer "overcoil" is wrapped around the hydrogel-covered coil [22]. Right, Posthydration image of the device, showing marked expansion of the hydrogel material, which has become translucent [22].

Spectra family microcoil is a platinum alloy wire wound into a primary coil which may contain either a polypropylene or an absorbable polymer and then woud into a secondary shape, spherical, complex or helical [21]. Spectra Bare Platinum coils (S-BP), belonging to Spectra family, have a primary outer diameter ranged from 10.5 um to 15 um which complex structure acting as scaffold for the inner core concentric filling favoring a high neck coverage and stability coiling reducing the use of stent [33]. The S-BP system is composed by three elements: a connecting cable, a Detachment Control Box (DCB) and a Microcoil System which includes a coil attached to a Device Positioning Unit (DPU), as seen in *figure 2.3* [21].

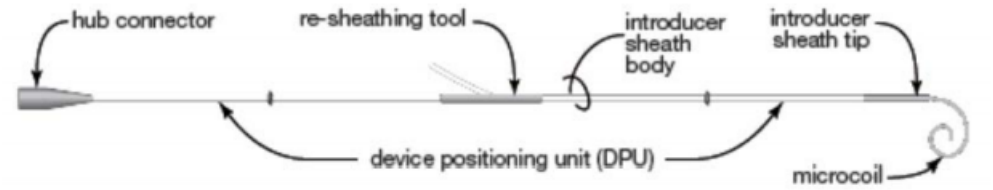

Figure 2.3: Microcoil System [21].

The Microcoil System is introduced in a sheath which provides protection to the coil in the packaging dispenser and also supports introduction of coil into the guide catheter [21]. The introducer sheath consists of three components: an introducer sheath tip, an introducer sheath body, and a re-sheathing tool [21]. The Detachment Control Box provides energy to induce the thermo-mechanical detachment of the coil from the device positioning unit and the energy is carried through the connection cable between the hub connector and the output connector on the DCB [21]. The DPU is a radiopaque wire that includes five markers used to indicate when the tip of the microcoil reached that of the microcatheter, a useful signal to insert new coils [21].

Chapter 3

Hemodynamic Analysis: Fluid-Structure-Interaction Simulation of a Brain Aneurysm

3.1 Introduction

Endovascular coiling treatment is one of the most widely used approaches for occluding cerebral aneurysms. The goal is to slow the blood flow velocity in the aneurysmal environment to induce clotting, reducing the rupture risk of the aneurysm. To predict clinical outcomes, doctors use Computational-Fluid-Dynamics (CFD)/ Computational-Structural-Dynamics (CSD) simulation or Fluid-Structure Interaction (FSI) simulation techniques, that are useful to better assess the hemodynamic characteristics of blood flow before and after treatment. Usually, the Newtonian blood behavior is taken into account which leads in particular to an overestimation of the blood velocity and a probable underestimation rupture risk. Hence, the need to investigate the non-Newtonian blood model and what effects it entails.
The focus of this chapter is the hemodynamic analysis of blood flow in an anatomically ideal model of a brain aneurysm and the changes due to the endovascular coiling treatment. The study conducted on the COMSOL Multiphysics platform, aims to evaluete the fluid-structure interaction in the case of untreated middle cerebral artery (MCA) aneurysm and in the case of treated aneurysm. In particular, in each case, a special attention has been placed on the influence of the blood rheology model: Newtonian and non-Newtonian blood. For the evaluation of the simulations, the following hemodynamic parameters of the blood flow have been analyzed:

- blood flow pattern,
- displacement,
- Von Mises stress.
- wall shear stress.

3.2 Geometry

The MCA aneurysm model studied is a simplified geometry, being an approximate patient-based computed tomography image reconstruction of a single segment of the middle cerebral artery with aneurysm, taken from [52]. The geometry has been built on COMSOL Multiphysics platform according to the reference geometry, neglecting the minor tortuosities of the Willis circle (*figures 3.1 a and b*), that is shown with blu highlight in *figure 3.1 b*. The geometric parameters of the MCA segment with aneurysm are shown in *table 3.1*. The wall thickness of the MCA alone has been hypothesized to be 0.3 mm (Torii et al., 2010 [53]). Abruzzo et al. [54] have demonstrated that the minimum thickness of an aneurysm prior to rupture is 0.05 mm, therefore it is considered a untreated thin-wall aneurysm whose thickness was set

to 0.10 mm. Both thicknesses are constant throughout instead of slightly becoming thinner as the radius of the real arterial tissue does. Aneurysm sac is modeled by a sphere with 5.6 mm in diameter that is located in a point of the MCA. For the treated aneurysm case, it has been assumed that the aneurysm sac is completely filled.

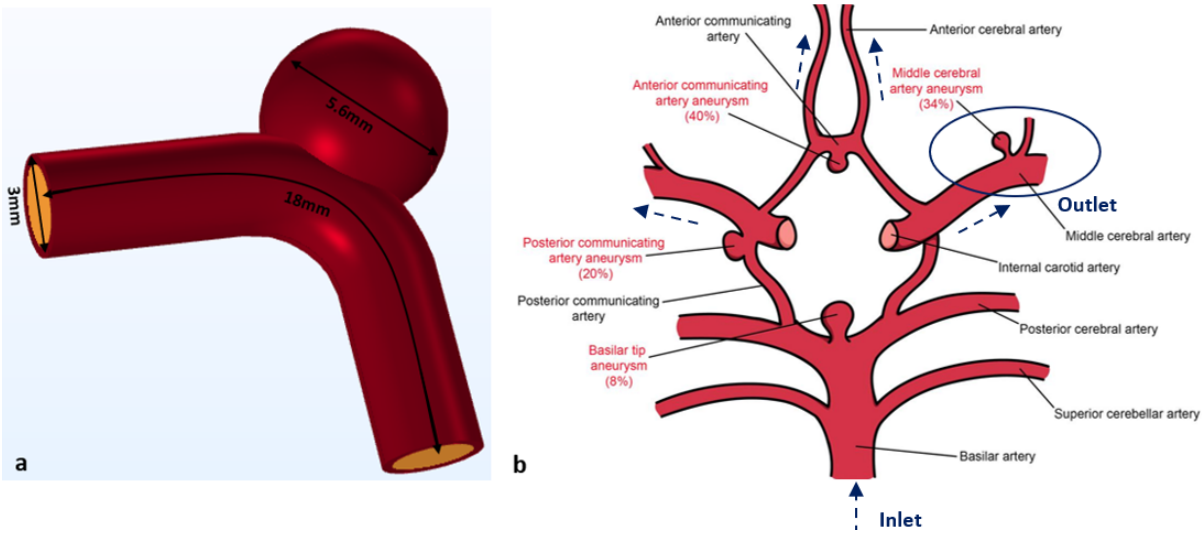

Figure 3.1: (a) Geometry of the Middle Cerebral Artery Aneurysm for the simulation. (b) The common sites of saccular aneurysms in the circle of Willis [50].

Table 3.1: Geometrical parameters of the MCA model.

Model Parameter	**Value**
Total length of the MCA	18.00mm
Arterial wall thickness	0.30mm
Outer diameter of the MCA	3.00mm
Aneurysm diameter	5.60mm
Aneurismal wall thickness	0.10mm

3.3 Blood: rheological properties and mathematical models

Blood is a fluid formed from a two-phases suspension of solid particles, i.e. red blood cells, white blood cells and platelets in a protein-rich aqueous solution called plasma [47]. The presence of these cells induces a non-Newtonian behavior linked to the percentage of hematocrit: for low values the viscosity that measures the resistance to blood flow is constant and equal to 3.5-4 mPa s, but for high values the shear-thinning behaviour of non-Newtonian blood is not negligible and the viscosity becomes a function of the shear-rate [47].
In the literature, blood has been studied as a non-Newtonian fluid according to the *Carreau-Yasuda* model or the *Casson* model or the *Herschel-Bulkley* model [49].
In this study the Carreau–Yasuda (CY) model has been implemented being widely used to describe the shear-thinning behaviour of blood in which the dynamic viscosity depends on the shear stress γ according to the equation (3.1): [48]

$$\eta_{app}(\gamma) = \eta_\infty + (\eta_0 - \eta_\infty) \cdot (1 + (\lambda\gamma)^\alpha)^{\frac{n-1}{\alpha}} \tag{3.1}$$

in which, η_0 and η_∞ are the zero-shear-rate and infinite-shear-rate viscosities, respectively; n is the power-law index which is dimensionless and λ is the time constant, calculated from the point on the dynamic viscosity curve where the blood flow transits from Newtonian region to the intermediate region. As shown in the *figure 3.2*, three different zones can be identified: a Newtonian region with η_0 for low shear rate, an intermediate region of shear-thinning in which η_{app} decreases with γ, a Newtonian region with a constant viscosity reached for high shear rates [46]. In this study the parameters values used, derived from Boyd et al. (2007) [48] which are reported in the *table 3.2*.

Table 3.2: Parameters values of the Carreu-Yasuda blood model.

Parameter	**Value**
η_0[Pa s]	0.16
η_∞[Pa s]	0.0035
λ[s]	8.2
α[1]	0.64
n[1]	0.2128

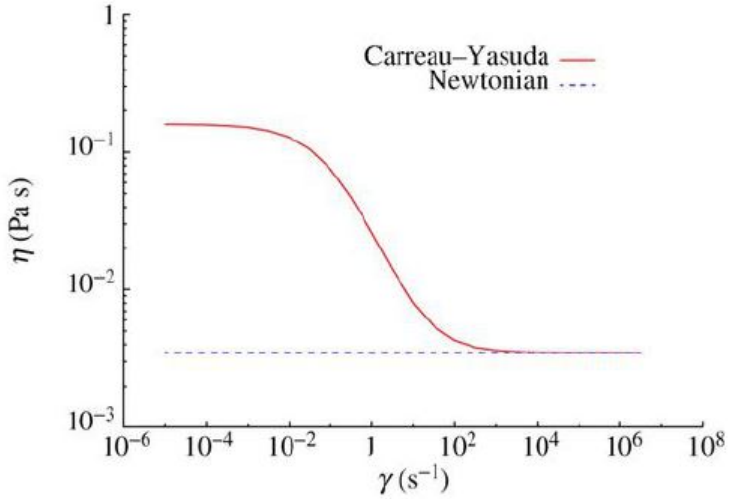

Figure 3.2: Dynamic viscosity as a function of shear-rate for the CY and the Newtonian models [46].

The comparatively Newtonian model is described by setting η_{app}=η_∞=0.0038 Pa s.
The incompressible blood flow through the MCA has been assumed to be stationary, laminar and three-dimensional. The model is described by the following *continuity* and *Navier Stokes* equations: [68]

$$\bigtriangledown \cdot u = 0 \tag{3.2}$$

$$\rho[\frac{\partial u}{\partial t} - u \cdot \nabla u] = \begin{cases} -\nabla p + \nabla \cdot (\eta \nabla u) + \rho g & \text{for Newtonian model} \\ -\nabla p + \nabla \cdot (\eta_{app} \nabla u) + \rho g & \text{for non-Newtonian model} \end{cases} \tag{3.3}$$

where u, ρ and p are the velocity, the blood density and the external pressure, respectively. The blood density was assumed to be costant ρ=1060 Kg m^{-3}.
The conservation equation of mass (3.2) indicates that the divergence of the velocity vector is zero at all points of the fluid volume considered. In the conservation of momentum (3.3) the inertia components are to the left and the divergence of stresses and external forces are respectively to the right.
To solve the fluid domain has been used the CFD module COMSOL Multiphysics, using a material sweep

with the two blood models, Newtonian model with constant dynamic viscosity, and a Carreau Yasuda model defined above. The *Join Dataset* functionality was used to compare both models.

3.4 Cerebral artery: rheological properties and mathematical models

Arteries and blood vessels in general are deformable solid domains composed mainly of collagen, elastin and smooth muscle cells [57]. The arteries are composed of three concentric layers: tunica intima, tunica media and tunica adventitia, which constitute the innermost, the intermediate and the outer layers respectively [57]. Arteries elastically dilate under the effect of blood pressure and subsequently contract, and this ability is known as vascular compliance. Hence, the need to introduce the effect of the fluid structure interaction that takes into account the vascular compliance phenomenon. The total thickness of the artery was considered without distinguishing the three concentric layers. Simplification has been adopted to reduce the long calculation time.
The MCA in this study has been modeled as a body with hyperelastic mechanical behavior including the tract where the aneurysm sac originates. Since the aneurysmal domain develops different rheological properties from the healthy artery domain as described by MacDonald et al. (2000) [66], it has been decided to use two different mathematical models for describing the hyperlastic materials of each subdomain. The *Neo-Hookean model* was used for the hyperelastic material of the middle cerebral arterial subdomain while the *Mooney-Rivlin model* was used for the hyperelastic material of the aneurysm subdomain. For a hyperelastic material, the stress–strain relationship derives from a strain energy function W [J m^3], which indicates the deformation state [57] (*Appendix A*). The strain energy of hyperelastic material is a function of the invariants of the Cauchy-Green strain tensor and in the Neo-Hooken model has the following form:[57]:

$$W = c_1(I_1 - 3) \tag{3.4}$$

with the material parameter c_1=$\frac{\mu_1}{2}$ and the first principal invariant I_1= λ_1^2+λ_2^2+λ_3^2 where λ_i are the principal stretches [57].

In the Mooney-Rivlin model the strain energy function using two invariants is the following:[57]

$$W = c_1(I_1 - 3) + c_2(I_2 - 3) \tag{3.5}$$

with the material parameters c_1=$\frac{\mu_1}{2}$ and c_2=-$\frac{\mu_2}{2}$ [57].

The parameters values used for this study are listed in the *table 3.3*.

Table 3.3: Subdomains Setting

Domain	Parameter	Value
Artery	Module	Solid Mechanics Module
	Material Model	Hyperelastic Neo-Hookean
	Density	ρ=960 kgm^{-3} [58]
	Lamè parameter (muLame)	$\mu = 6.20e^6 Nm^{-2}$ [58]
Aneurysm	Module	Solid Mechanics Module
	Material Model	Hyperelastic Mooney-Rivlin
	Density	ρ=960 kgm^{-3} [58]
	Material parameter	c_1=15 Ncm^{-2} [57]
	Material parameter	c_2=4 Ncm^{-2} [57]

3.5 Boundary Conditions

In this study, a velocity and a pressure profile in the MCA have been used as the inlet and outlet boundary conditions, respectively. The blood velocity flow has been reproduced from Liu et al.(2015), that have been collected Transcranial Doppler (TCD) signals of patients with suspected cerebrovascular disease [51]. The velocity waveform has been constructed as an eighth-order Fourier function that generalizes the TCD waveform of all patients, applying Parseval's theorem to such periodic signals whose individual Fourier components are summed as follows: [51]:

$V(t) = 64.5 - [5.154\cos(7.85t) - 10.962\sin(7.85t)] - [5.4516\cos(2*7.85t) - 1.7574\sin(2*7.85t)] - [1.731\cos(3*7.85t) + 0.846\sin(3*7.85t)] - [1.5684\cos(4*7.85t) + 0.23976\sin(4*7.85t)] - [0.50328\cos(5*7.85t) + 1.0524\sin(5*7.85t)] - [0.10014\cos(6*7.85t) + 0.30504\sin(6*7.85t)] - [0.035316\cos(7*7.85t) + 0.3963\sin(7*7.85t)] + [0.16248\cos(8*7.85t) - 0.17118\sin(8*7.85t)]$.

As can be seen clearly in the *figure 3.3 a*, a cardiac cycle of about 0.8 s was considered.
The output boundary condition is based on the cerebral pressure profile shown in *figure 3.3 b*, which was taken from the "PhysioNet" IT platform which makes the collected EEG signals available.

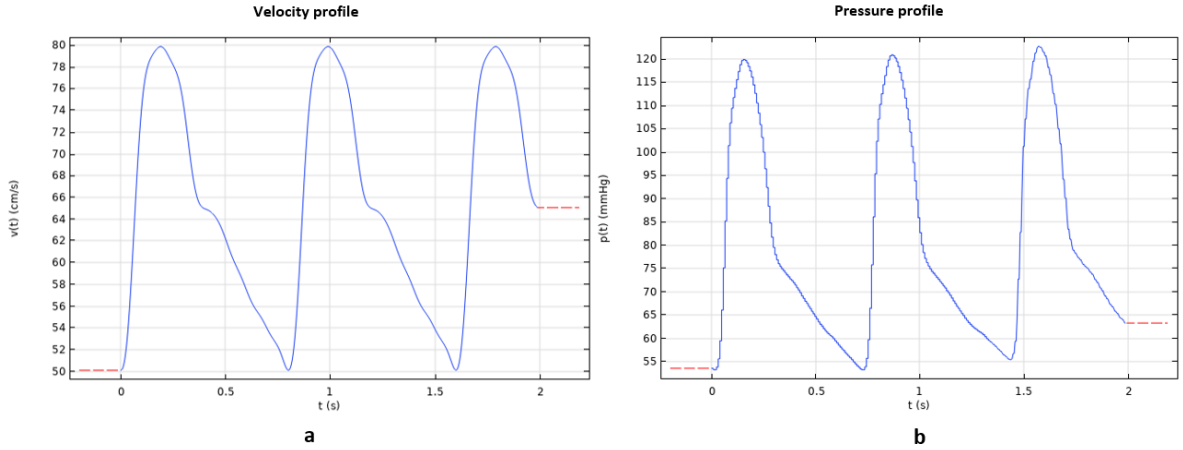

Figure 3.3: Boundary Conditions:(a) Velocity profile at the inlet.(b) Pressure profile at the outlet.

Displacements and tractions at the blood-artery interface were set equal and opposite according to the equations (3.6) and (3.7). No-slip boundary condition has been imposed for the vessel and aneurysm walls (equation (3.8)).

$$d_b = d_a \tag{3.6}$$

$$n_b \cdot \sigma_b = n_a \cdot \sigma_a \tag{3.7}$$

$$\dot{\sigma_b} = \dot{\sigma_a} \tag{3.8}$$

where d, σ and n are the displacement, stress tensor and the normal vector of the boundary surface. The subscripts b and a refer to blood and artery, respectively.

3.6 Mesh

The governing equations were solved using the *Finite-Element Method* (FEM). In this research, the fluid and solid domains have been discretized using tetrahedral mesh elements . The mesh for the solid domain consists of 18,684 nodes and 60,322 elements, whereas the fluid domain mesh contains 50,630 nodes and 278,859 elements. The total domains elements mesh are presented in *table 3.4*. A fine type mesh has been used for both domains. The solid domain mesh is shown in *figure 3.4*.

Table 3.4: Domains elements mesh

Domain	Parameter	Value
Solid domain	Number of elements	$60,322$
	Number of nodes	$18,684$
	Minimum element quality	0.212
	Average element quality	0.7083
	Element volume ratio	0.004061
	Mesh volume	$48.49mm^3$
Fluid domain	Number of elements	$278,859$
	Number of nodes	$50,630$
	Minimum element quality	0.1944
	Average element quality	0.6644
	Element volume ratio	0.002416
	Mesh volume	$154.9mm^3$

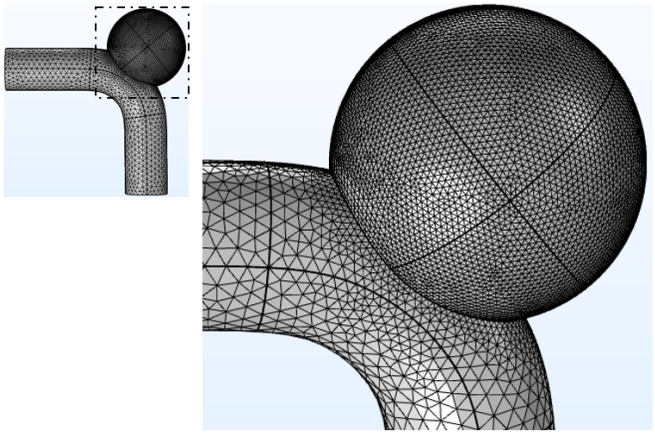

Figure 3.4: Solid domain mesh.

The FEM discretizes each domain with a thickening of the grid in the vicinity of obstacles, such as curves, aneurysm in order to return a more accurate solution. A fundamental parameter that reads the discretization grid quality is expressed as follows:[59]

$$q = \frac{72\sqrt{3} \cdot V}{\sqrt{(h_1^2 + h_2^2 + h_3^2 + h_4^2 + h_5^2 + h_6^2)^3}} \tag{3.9}$$

in which V is the discretized volume and h_1, h_2, h_3, h_4, h_5, h_6 are the lengths of the sides of the discretization tetrahedral elements and q should be above 0.2 for a good mesh [59].
In order to obtain an accurate solution of the current FSI simulation, it is necessary introduce some mesh thickening parameters near the obstacles to the blood flow, defining the maximum and minimum size of the mesh element and the growth rate, which have been setted equal to 0.468 mm, 0.0884 mm and 1.13 respectively.

3.7 FSI simulation

In the hemodynamic analysis, the vascular compliance effect, due to the interaction between the wall of the aneurysm and the blood, must also be taken into account. This can be simulated with the FSI tool. COMSOL solver allows to simulate the FSI problem combining and solving two physics simultaneously: fluid flow which studies the blood flow velocity and cerebral pressure fields inside the MCA, which become the inputs for the solid mechanics that returns the deformations and stresses on the arterial and aneurysmal walls [60].
The FSI simulation uses the *Arbitrary Lagrangian-Eulerian* (ALE) finite element method for studying the solid and fluid interaction. It is a combination of the Eulerian description of the blood flow where the mesh node is held fixed and the Lagrangian description where the mesh node follows the material point [60].
Indicating the boundaries between artery and blood as couplings, the coupled FSI problem can be one-way or two-way. In the *one-way FSI simulation* only the fluid domain data is transferred to the solid domain, unlike the *two-way FSI method* in which the resulting fields values of the solid domain, in turn, become the inputs of the fluid domain and on the basis of which, the solver modifies the mesh using it for the next iteration and so on until it reaches convergence [60]. In this study a one-way FSI was performed to reduce the longer calculation time. Therefore, the one-way FSI simulation is suitable for very small structural displacements. It sequentially solves the fluid flow using the continuity (3.2) and Navier-Stokes (3.3) equations, computes the fluid load at the interface according to the eqaution (3.10) and then uses it for computing the solid displacements [60]. The blood force exerted on the arterial wall boundary is the negative of the reaction force on the blood: [60]

$$f = n \cdot [-pI + (\eta(\bigtriangledown u + (\nabla u)^T) - \frac{2}{3}\eta(\bigtriangledown u)I)] \tag{3.10}$$

in which p indicates pressure, η and u are the dynamic viscosity and the blood velocity, n the outward normal to the boundary and I the identity matrix [60].

The process steps are depicted in the *figure 3.5*.

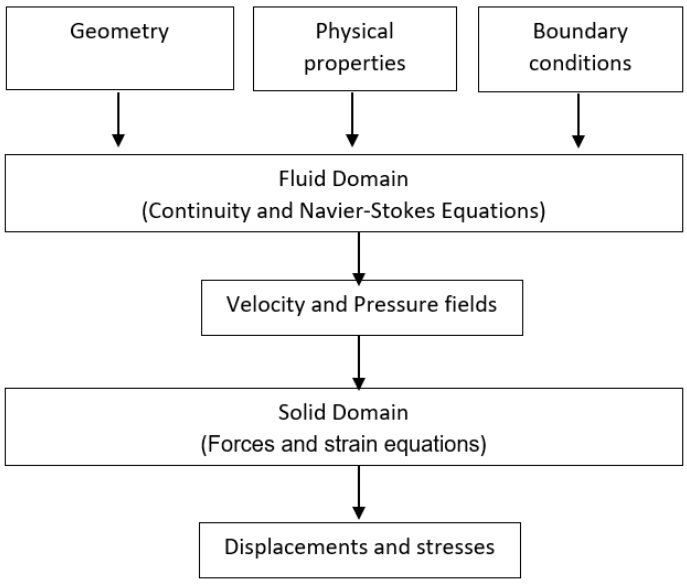

Figure 3.5: Steps of the one-way FSI method.

3.8 Results

The Newtonian and non-Newtonian simulations were studied for the purpose of observing the main differences that are generated by not considering the dynamic changes in blood viscosity. The results are reported in both models for the untreated aneurysm case, while for the treated case they are discussed only for the non-Newtonian model, because it was considered the most complete.

3.8.1 Pressure and velocity profiles

Figure 3.6 shows the pressure distribution over the artery and aneurysm. There are a pressure drops in the direction of the flow and is $\sim$ 0.6 KPa between the inlet and outlet in both models. The pressure distribution on aneurysm sac is constant.

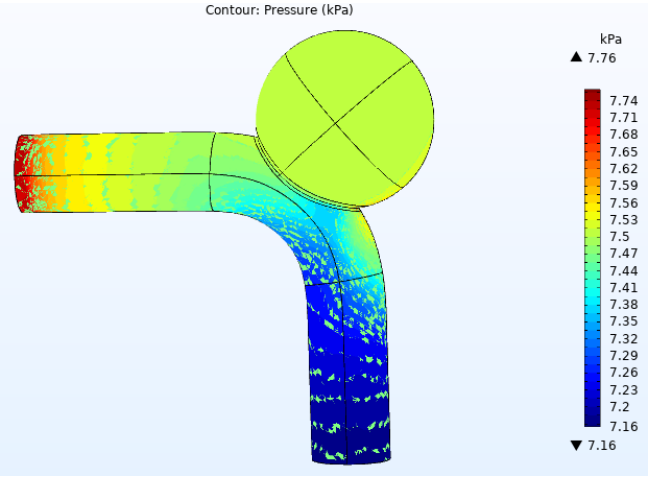

Figure 3.6: Carreau-Yasuda model. Pressure distribution.

The description of blood behavior using the Carreau Yasuda model produced a dynamic viscosity ranging from 3.5 mPa s to 9.4 mPa s (see *figure 3.7*). Also the shear rate range is slightly narrow, therefore the velocity profiles differ.

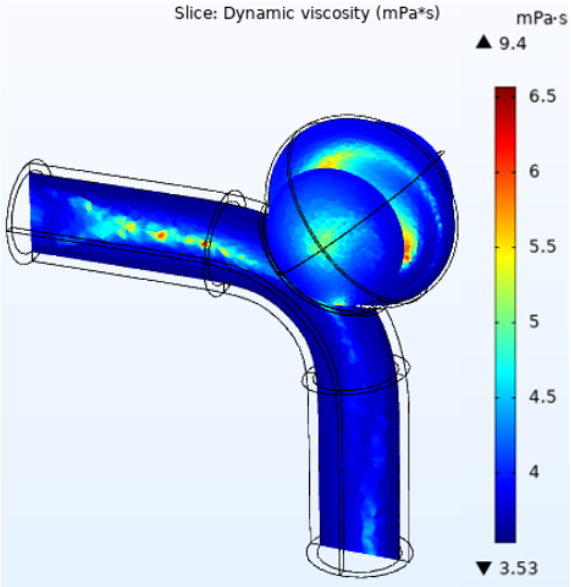

Figure 3.7: Carreau-Yasuda model. Dynamic viscosity.

In *figures 3.8 a and c* the blood flow patterns have been shown in x-y midplane for the Newtonian and non-Newtonian models. The velocity inside the aneurysm sac for the two cases has been shown in *figures 3.8 b and d*. In general, it is seen how the blood flowing down the artery, penetrates the aneurysmal sac going to the right side of the wall according to the flow direction. Within the aneurysm, the blood flow slows down and its conflict with the wall causes the formation of a vortex flow as shown in *figure 3.9*. The maximum velocity at the aneurysm neck equals to 72.3 $\mathrm{cm}s^{-1}$ and 71.8 $\mathrm{cm}s^{-1}$ for the first and second models, respectively. The magnitude velocity on the central plane of the aneurysm is lower than the maximum velocity reached at the aneurysm neck. The low amount of blood flow that enters into the aneurysm leads to a low shear stress on the aneurismal wall. The area with vortex flow is characterized by a lower shear stress which induces the creation of stagnation points more vulnerable to the aneurysm rupture than the other points.

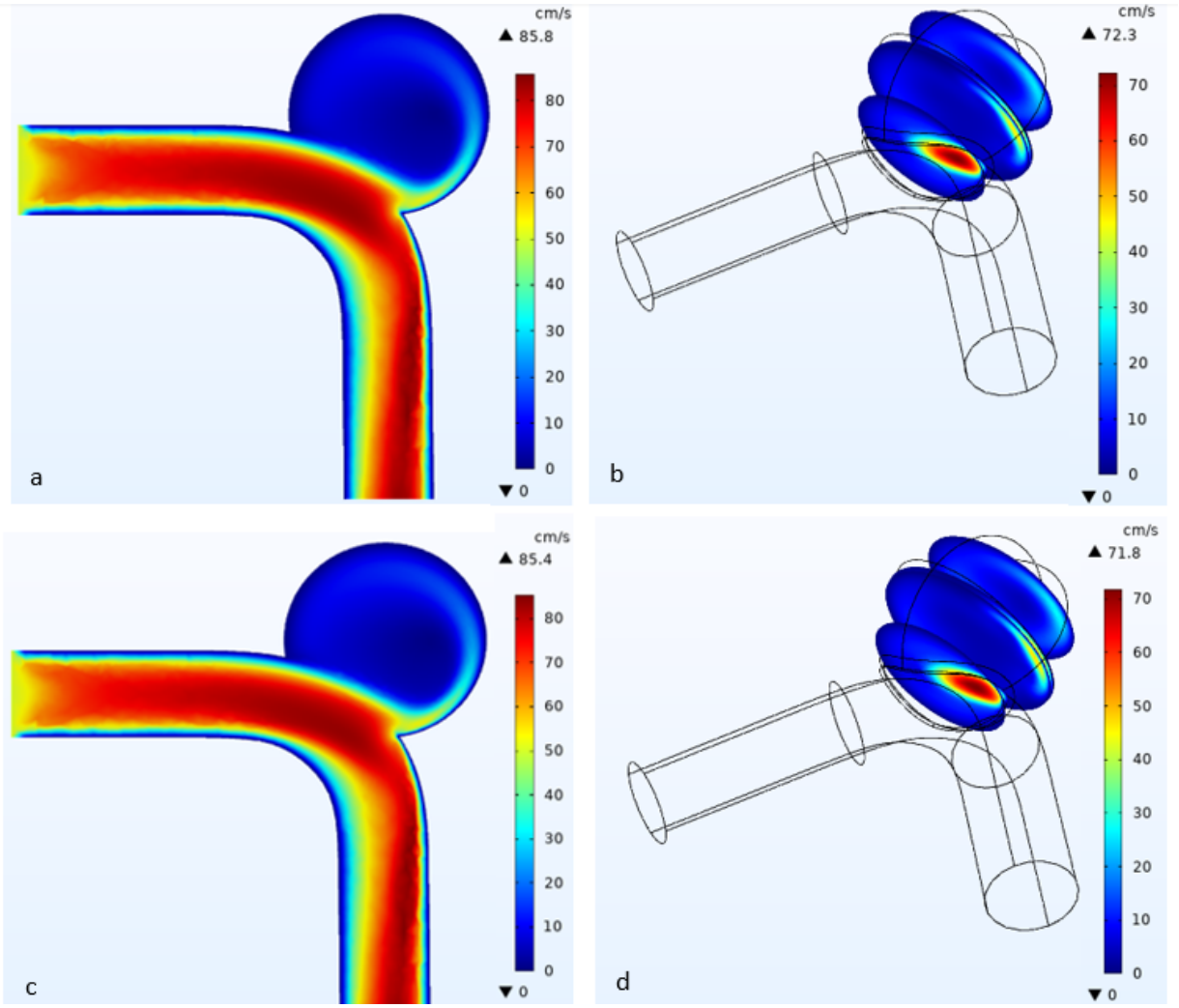

Figure 3.8: Velocity flow: (a) Newtonian blood through MCA with aneurysm. (b) Newtonian blood inside the aneurismal sac. (c) Non-Newtonian blood through MCA with aneurysm. (d) Non-Newtonian blood inside the aneurismal sac.

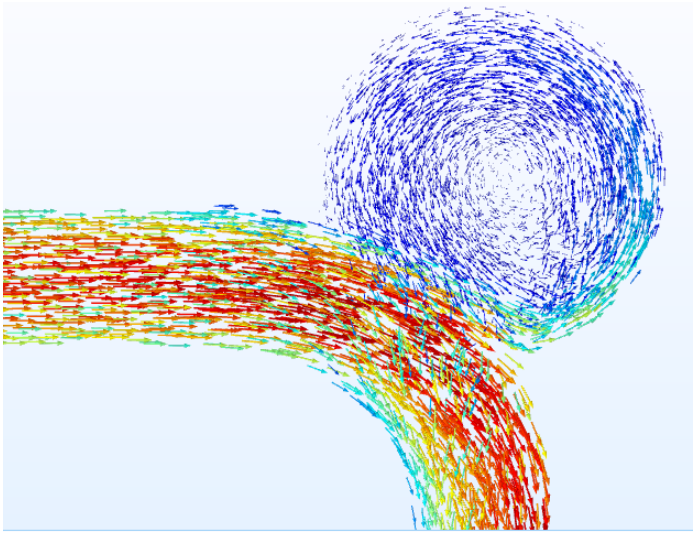

Figure 3.9: Carreau-Yasuda model. Velocity vectors in the weakening point and aneurysm sac.

Although the flow pattern velocity in Newtonian model doesn't differ much to the non-Newtonian one, it causes the overestimation of velocity blood and consequently the underestimation of the rupture risk. The relative difference regarding the blood velocity is shown in detail in *figure 3.10*. The results of the two different viscosity models for blood behavior showed differences in the estimate of hemodynamic up to a surplus of 1.23 cm s^{-1} relative to velocity. *Table 3.5* compares the values of characteristic quantities within the aneurysm sac in the Newtonian model and Carreau-Yasuda model.

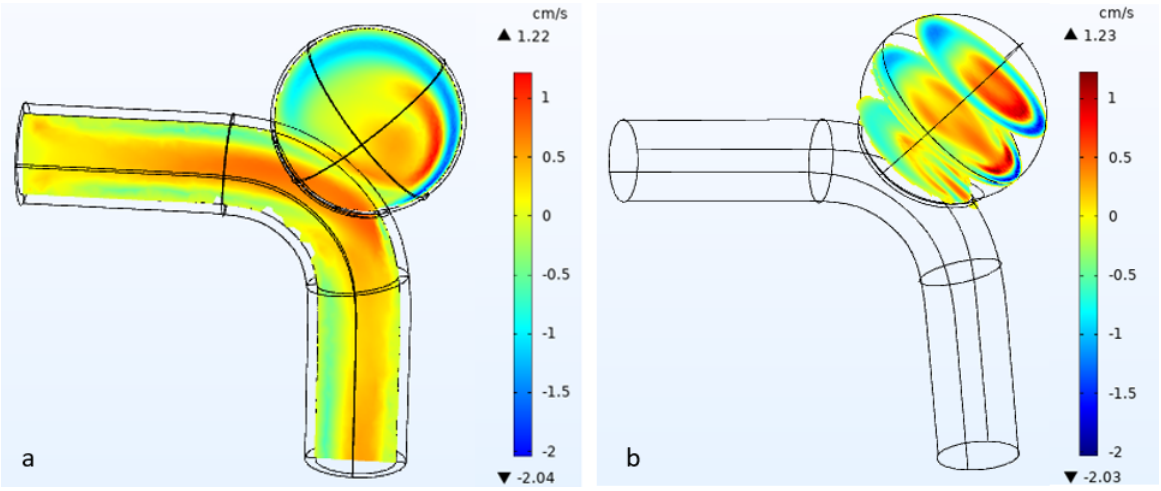

Figure 3.10: Relative velocity differences:(a) through MCA with aneurysm; (b) inside the aneurysm sac.

Table 3.5: Relative hemodynamic changes to the Newtonian model within the aneurysm sac.

Parameter	**Newtonian**	**Carreau-Yasuda**
min viscosity[mPa s]	3.89	3.53(−9.3%)
max viscosity[mPa s]	3.89	9.4(+141.7%)
min shear rate[s^{-1}]	10.7	13.8(+28.9%)
max shear rate[s^{-1}]	5,670	5,810(+2.5%)
max velocity[cms^{-1}]	72.3	71.8(−0.7%)

For treated aneurysm case, how it is seen in *figure 3.11*, the endovascular coiling treatment removed the vortex flow and the blood inflow in the aneurysm sac.

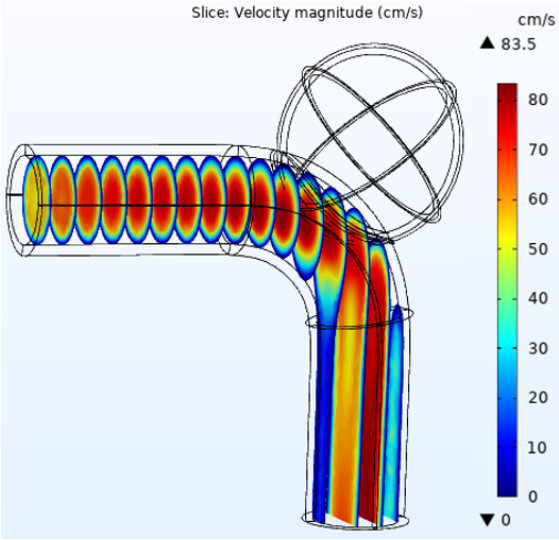

Figure 3.11: Treated aneurysm: Velocity profile of the Carreau-Yasuda model.

3.8.2 Displacements

Figures 3.12 a and b show the wall displacements distribution in the untreated and treated aneurysms, respectively. Since no significant differences appear for the total wall displacement in the untreated case when the results between the two blood models are compared, only those of the Carreau-Yasuda model are reported. For the untreated case (*Figure 3.12 a*), it can be seen that the maximum displacement occurs around the aneurysm neck. The maximum displacement equals to 2.29 μm and 0.52 μm for the first and second cases, respectively. In the treated case, the displacement (*Figure 3.12 b*) is lower relative to the untreated case, due to the blood flow pattern change. The maximum displacement for the treated aneurysm is 77% less than the untreated case and likewise it is close to the point of curvature of the artery. Therefore, the endovascular coiling treatment involves a wall displacement reduction lowering the rupture risk.

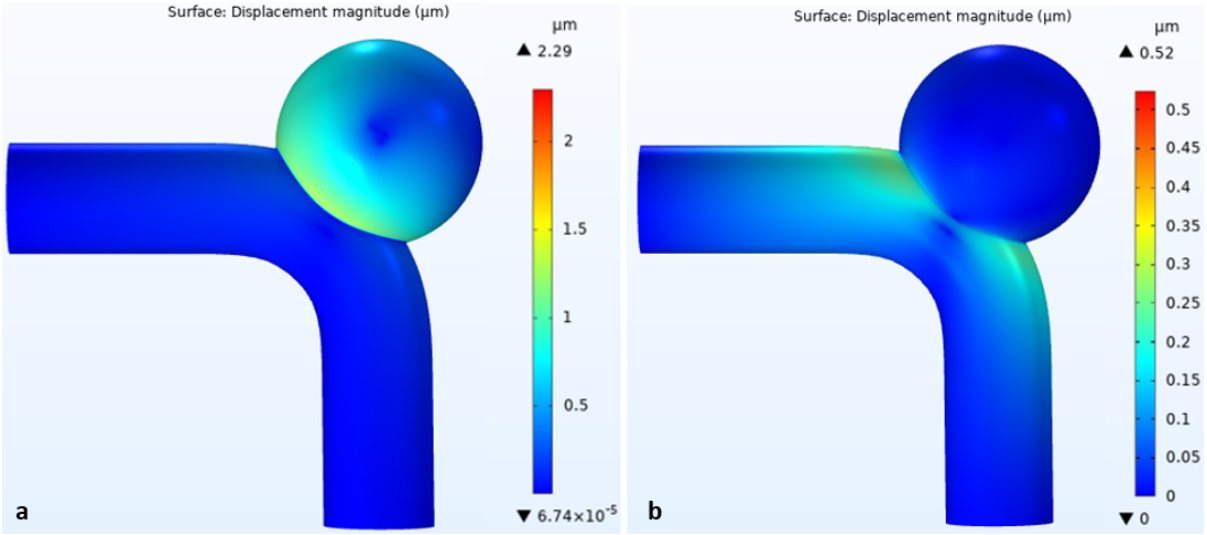

Figure 3.12: Carreau-Yasuda model. The displacement contour: a) Untreated aneurysm. b) Treated aneurysm.

3.8.3 Von Mises stress

The Von Mises Stress distribution on the arterial and aneurismal walls have been shown in the *figure 3.13*. It is seen there is a strong correlation between the wall displacement and von Mises stress. Von Mises stress is a combination of the normal and shear stresses exerted on the solid domain and this parameter is used to describe the yielding of a material which in this study coincides with the rupture of the aneurysm. The expression of Von Mises stress (σ_{VM}) contains the principal stresses according the equation (3.11):[56]

$$\sigma_{VM} = \sqrt{\frac{1}{2}[(\sigma_1 - \sigma_2)^2 + (\sigma_2 - \sigma_3)^2 + (\sigma_3 - \sigma_1)^2]} \tag{3.11}$$

in which σ_1, σ_2 and σ_3 are the principale stresses.
For both models, the maximum Von Mises stress occurs at the maximum displacement, the aneurysm neck. The maximum Von Mises stress magnitude for Newtonian and Carreau-Yasuda models are 87.8 kPa and 87.5 kPa, respectively. The maximum relative difference of 64% (see *figure 3.13 c*) is observed between the two models at the aneurysm neck. Therefore, the blood viscosity slightly affects the Von Mises stress magnitude. In the treated aneurysm, as can be seen in *figure 3.14* the curve of the artery was confirmed as the highest maximum stress area with the relative reduction equal to 17%.

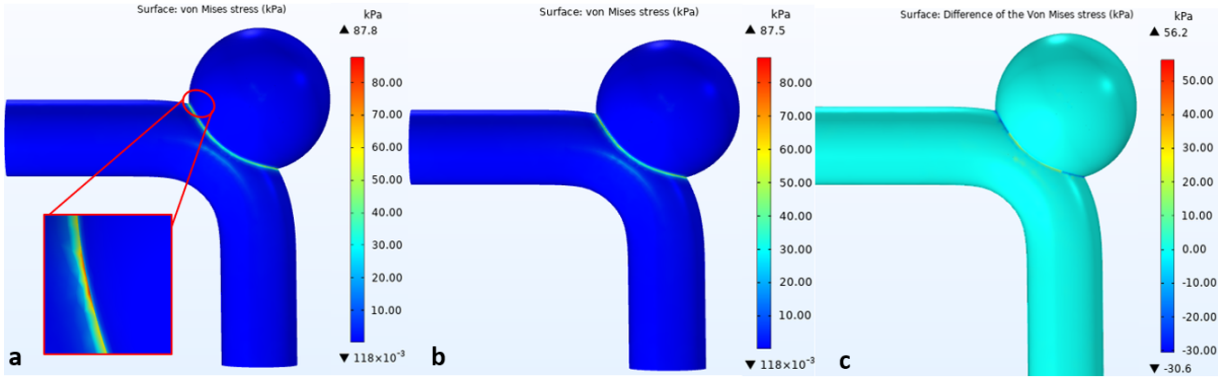

Figure 3.13: The Von Mises stress distribution in the untreated aneurysm: a) Newtonian model. b) Carreau-Yasuda model. c) Relative difference.

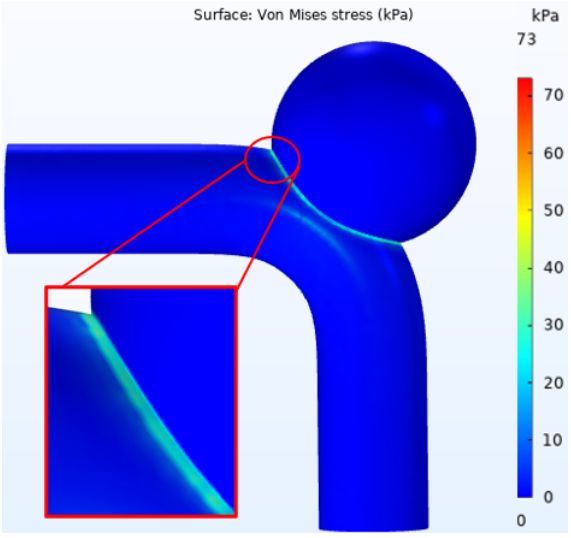

Figure 3.14: Carreau-Yasuda model. The Von Mises stress distribution in the treated aneurysm.

3.8.4 Wall shear stress

Wall shear stress (WSS) is a flow-induced stress and is defined as the frictional force of viscous blood tangential to the arterial wall. So, this parameter is an indirect measure of dynamic viscosity. Multiple studies have been demonstrated how the WSS affects the degradation of endothelial cells and their death, and therefore the rupture risk of the aneurysm. *Figures 3.15 a and c* show the WSS distributions in the complete geometry. As can be seen, in both models, the lower wall shear stress occurs on the aneurysm. Those low WSS values are a consequence of slow blood flow inside the aneurysm sac. The maximum WSS magnitude is 24.5 Pa for the Newtonian model and 21.8 Pa for the Carreau-Yasuda model. *Figures 3.15 b and d* show in detail the wall shear stress in the aneurysm only. It can be seen that the dominant range of wall shear stress on the aneurysm sac varies from 0.04 Pa to 5 Pa, with the exception of that on the aneurysm neck, from which the blood flow enters, where the highest values are reached. It was also found that there is a strong dependence of wall shear stress on blood viscosity, since an increase in viscosity causes an overestimation of the WSS peak value. *Figure 3.16* shows how the low wall shear stress area on aneurysm has been removed by endovascular coiling treatment.

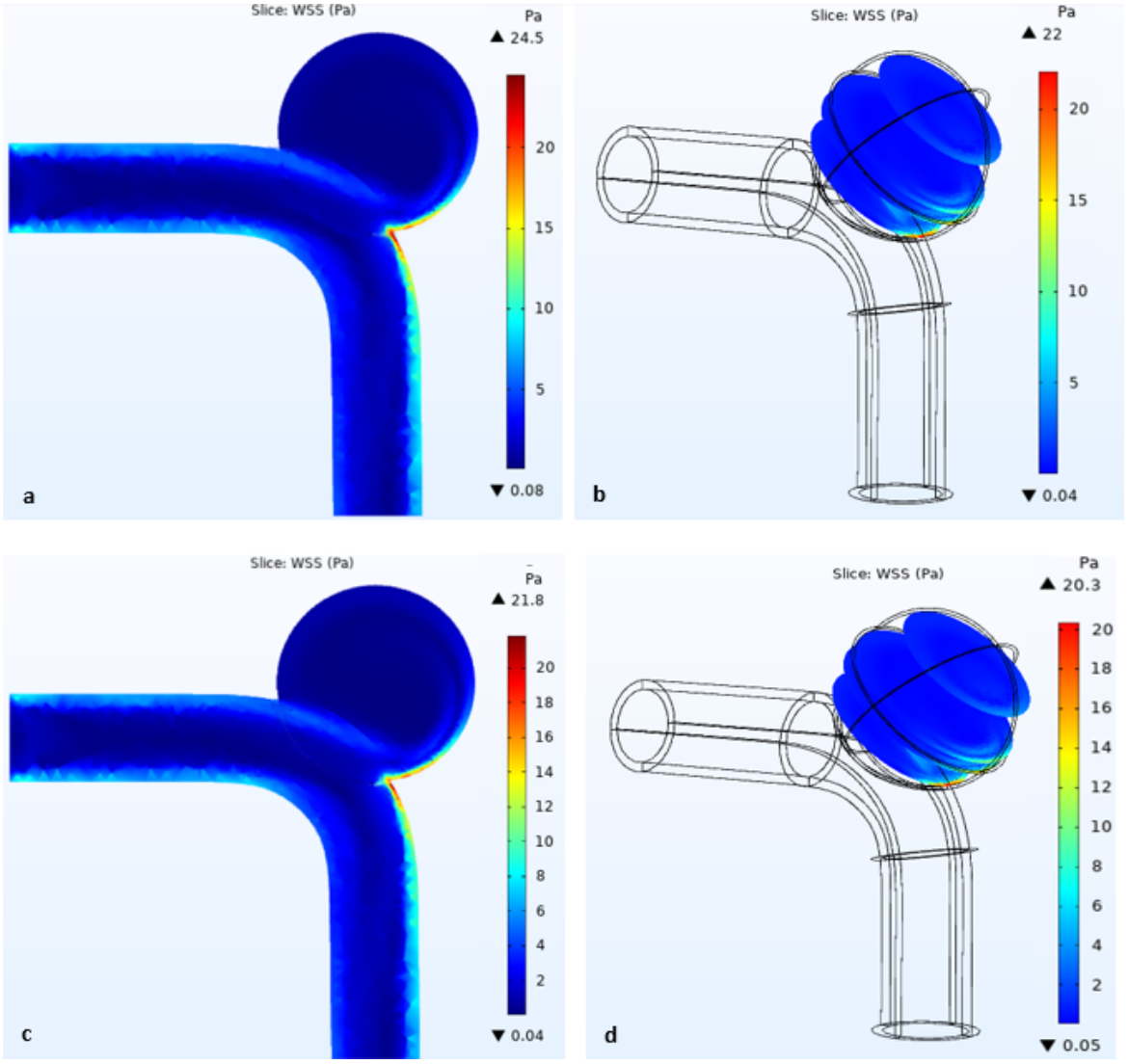

Figure 3.15: (a) WSS distribution on MCA with aneurysm (Newtonian model). (b) WSS distribution in the lower, middle, and upper planes inside aneurismal sac (Newtonian model). (c) WSS distribution on MCA with aneurysm (Carreau-Yasuda model). (d) WSS distribution in the lower, middle, and upper planes inside aneurismal sac (Carreau-Yasuda model).

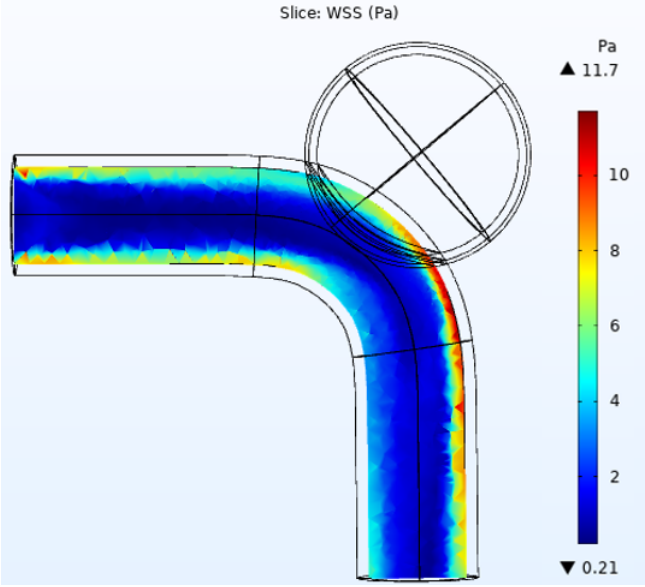

Figure 3.16: Carreau-Yasuda model. The WSS distribution in the treated aneurysm.

3.9 Discussion

Fluid Structure Interaction simulation represents a powerful tool for studying and quantifying hemodynamic outcomes in an anatomically ideal model of a brain aneurysm and the effects of endovascular coiling treatment. FSI performed prior to surgery helps to predict clinical outcomes and further complications and thus can reduce the risk of mortality and morbidity of the surgery. Typically, the hemodynamic parameters used in the studies are: the velocity vectors and the number of flow vortices, the wall shear stress, the effective stress. Of interest is the number of vortices that form in the aneurysm sac and that describes the changes in flow properties that occur in the presence of a brain disease. Xiang et al. (2011, [62]) reported a strong correlation between two or more vortices in the aneurysm sac with a high risk of aneurysm rupture, demonstrating that unruptured aneurysms had a single vortex. In the results obtained in this study, as shown in *figure 3.9*, a single vortex is formed in the aneurysmal environment, therefore the probability of aneurysm rupture risk is very low and as can be seen in the *figure 3.11* the vortex in the treated aneurysm is removed thanks to the endovascular coiling treatment. Furthermore, Hoi et al. (2006, [63]) reported that blood flow enters the aneurysm sac from the distal neck and, forming a vortex, exits the proximal neck. This blood flow pattern is confirmed in this research (see *figure 3.9*). The WSS parameter is studied because it influences the formation of the aneurysm and the rupture risk. The maximum values of WSS occurring in a cerebral artery with aneurysm reported in the literature vary between 30 Pa [64, Lu et al., (2011)] and 60 Pa [61, Castro et.al (2006)]. In this study the maximum WSS equals to 24.5 Pa which is below the indicated upper limits. Obviously, the influence of the ideal geometry used is to be considered and patient-based geometry could be used as the next step to obtain more accurate results. Shamloo et al. (2017, [60]) reported that the range of wall shear stress achieved on the aneurysm dome varies from 0.05 Pa to 2.5 Pa due to lower velocities, which are in accordance with the results of this study. WSS can increase or decrease owing the velocities and viscosities. Razavi et al. (2018, [67]) studied hemodynamics in MCA using both the Newtonian model and the Carreau-Yasuda model for non-Newtonian blood. They reported a greater influence of the blood rheological model on the wall shear stress profiles than the velocity profiles, as WSS are directly dependent on blood viscosity. Furthermore, they stated that the Newtonian model can only be accepted in CFD analysis, therefore having performed a FSI analysis in the current study, both models were compared. A greater deviation in the WSS values obtained is confirmed. The WSS values are also influenced by the arterial model adopted. Since the structural properties in the aneurysm dome differ from those of the arterial wall as reported by MacDonald et al. (2000, [66]) and that the rigid arterial wall hypothesis, as stated by Isaksen et al. (2008, [65]), leads to an overestimation in the WSS, in this study, two different hyperelastic models have been used to describe the elastic properties of the aneurysmal and arterial tissues. The Mooney-

Rivlin model with two material parameters is used to describe aneurysmal wall, while the Neo-Hookean model with only one material parameter is used to describe the arterial wall. The latter although is more accurate than the mechanical behavior of the artery described using a linear elastic model, it results less precise than model used for the aneurysmal wall. These choices were made to reduce the long calculation time.
In the hemodynamic analysis another important parameter to take into account is the Von Mises stress, which predicts the aneurysm rupture. It was stated that the area with maximum stress and deformation represents the rupture point in cerebral aneurysm. MacDonald et al. (2000, [66]) reported that the tissue rupture stress of the brain aneurysm ranges from 1.09 MPa to 1.91 MPa. In this study the obtained Von Mises stress is 0.088 MPa and 0.073 MPa for the untreated and treated aneurysm, respectively, concluding that the probability of rupture is very low. According to Shamloo et al. (2017, [60]) and Isaksen et al. (2008, [65]), the maximum Von Mises stress occurs at the neck of the aneurysm and this also finds correspondence in the current study as can be seen in the *figure 3.13*.
The anatomical simplifications in the geometry of the artery place a strong limitation on the model. First, an ideal geometries of the MCA and the aneurysm were constructed, neglecting their real asymmetry to avoid the large number of non-linear effects, that means expensive computational calculation. The minor tortuosities were omitted with consequent underestimation of the blood flow supply, and the total thickness of the artery was considered without distinguishing the three concentric layers. A next step could include a patient-based model with multilayer arterial wall to better estimate the clinical outcomes of endovascular coiling treatment.
A final limitation is represented by the stationary study performed. The ideal is to study the FSI problem as a function of time, in order to consider the most significant results achieved during the systolic peak. This was not done due to the lack of the high memory capacity required by the time-dependent study. In a time-dependent study only the magnitude of the results would change, but not their distribution.

Chapter 4

Coils Families used in Endovascular Treatment of Cerebral Aneurysm: A Cost-utility Analysis

Coiling endovascular therapy has been shown to be safe and clinically effective for the treatment of brain aneurysm, as well as being the least invasive. Nowadays, there are many types of cerebral coils available commercially that differ in shape and material. However, the economic impact of these different types of coils has not been established. Hence the need to conduct an economic health analysis.

4.1 Pharmacoeconomics

The health economic is the science that deals with the evaluation of the costs and benefits of the health system [26].
Pharmacoeconomics is a branch of the health economic which compares a pharmacological treatment for a given clinical condition to another [26]. The evaluation of a pharmacological strategy revolves around the following aspects:[26]

- *safety*, index that takes into account the related side effects due to the treatment followed;
- *clinical efficacy*, is the clinical value, the result of clinical studies which dictates the presence or absence of an improvement due to the administration of the therapy;
- *effectiveness*, is the medical value, extracted from the clinical results which reflects the clinical advantages resulting from the therapy;
- *utility*, patient satisfaction with regard to improving the quality of life;
- *costs*, consumption of resources in relation to the clinical benefits deriving from the treatment.

These aspects are accompanied by *allocative efficiency*, that is the ability to best distribute the available resources among the various alternative therapeutic treatments to obtain the best clinical result studying the relationships between *costs (inputs)* and *consequences (outcomes)* of one or more strategies and their impact on the stakeholders from patients to health system and society [26].
Therefore the pharmacoeconomics allows to identify, through the comparison of various alternative pharmacological treatments, that with the best cost-benefit ratio in relation to efficacy [26].
In this project, the health economic analysis aims to compare two families of cerebral coils:

- Spectra Bare Platinum Family coils whose particular structure reduces the additional use of the stent;
- All the other coils on the market, which often require the support of the SAC or BAC technique.

A general scheme of the analyzed problem is represented in the *figure 4.1.*

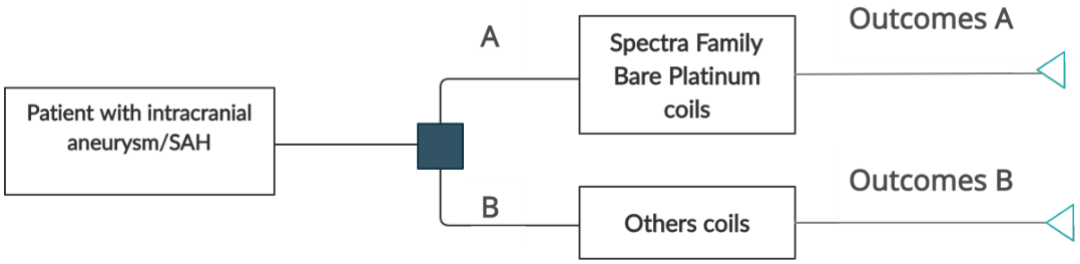

Figure 4.1: The therapeutic strategies of economic evaluation.

4.2 Components of an economic health evaluation

4.2.1 Costs

Costs used in pharmacoeconomics are divided into:[26]

- *direct*;
- *indirect*;
- *intangible*.

Direct costs are related to the goods and services provided for a treatment and can be: [26]

- *direct medical costs*: are the expenses of the national health system or of third-party payer and include hospitalization of the patient, medicines and medical supplies, diagnostic tests, surgical interventions;
- *direct non-medical costs*: are the expenses associated with the resources employed of a non-medical nature borne by the patients such as means of transport or the transfer from the hospital to home.

Indirect costs reflects the loss of productivity due to the disease and can be: [26]

- *indirect medical costs*: costs of the treatment program incurred by the patient for survival;
- *indirect non-medical costs*: reflect the value of the resources not produced due to illness such as lost working days, the deterioration of the patient's quality life or the grade of the subject's disability.

Intangible costs, on the other hand, are associated with pain and psycho-physical discomfort deriving from the disease [26].

4.2.2 Outcomes

The term *outcome* reflects the end results of a therapeutic treatment and can be *economic*, *clinical* or *humanistic* [26].
Economic outcomes are the resources employed in a therapeutic treatment or alternative program and the associated costs [26].
The clinical outcomes of patients can be expressed through objective *physiological variables* such as reduction in blood pressure or through *humanistic endpoints* such as quality of life, patient satisfaction that take on a subjective character because strictly linked to the life's perception of the individual patient [26].
Quality of life measurement is an attempt to measure the results of a clinical treatment. Quality of life is a multidimensional concept that measures health condition and its impact on life conditions including

family, work, social and psycho-physical state [26]. Certainly medical treatment affects *health-related quality of life* (HRoL) which in pharmacoeconomics becomes a measure of the outcomes reported by the patient himself. One of the main indicators of quality of life is *Quality Adjusted Life Years* (QALY) [26]. QALYs express the benefit of a treatment and are the product between the utility (U) for a given health state and years of stay in it (Y): [26]

$$QALY = U * Y \tag{4.1}$$

The utility associated with a perfect health state is 1, 0 for the death state and a value between 0 and 1 for a reduced health state [26]. QALYs are a representative measure of outcomes that combines the gains of quantity and quality of life as shown in *figure 4.2* where the blue zone indicates the years in which the patient would have remained alive without following the treatment, while the gray zone indicates the lengthening of life following the therapy [26].

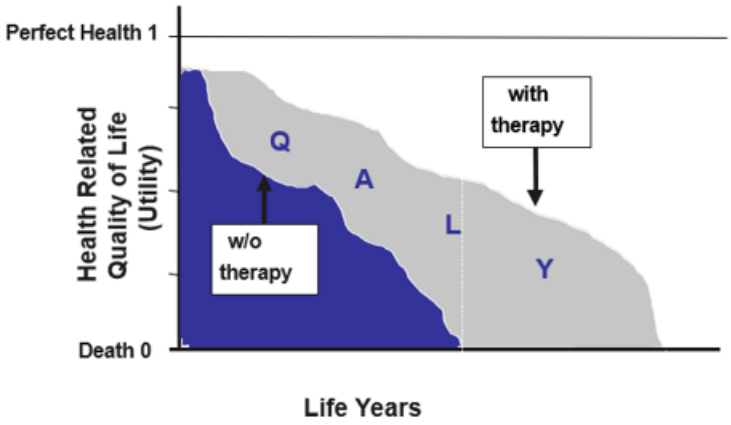

Figure 4.2: Quality-adjusted life years gained from an intervention [26].

Three methods can be used to assign utility to each health state: [35]

- *Rating scale*,
- *Time trade off*,
- *Standard gamble*.

The Rating Scale is the simplest method based on graded scales such as the *Visual Analogue Scale* (VAS) [35]. With this scale the patient is asked to indicate on a segment 100 mm long a point corresponding to own health condition at the time of assessment and then this point is reported to values between 0 and 1 as shown in *figure 4.3* [35].

Figure 4.3: Visual Analogue Scale [35].

In the Time trade-off method, patients are asked to imagine leading a life as a survivor of a specific chronic disease, brain aneurysm for the current study, and how many years of life they would be willing to give up in order to live in perfect health. The question is repeated with a life span in perfect health 'X' that is always shorter than the remaining life span "T" in a ill state, until the two alternatives will be indifferent [35]. The value of the utility is the ratio of "X" to "T" [35]. An example of Time trade-off with the coiling endovascular treatment as a theme is shown in the *figure 4.4*.

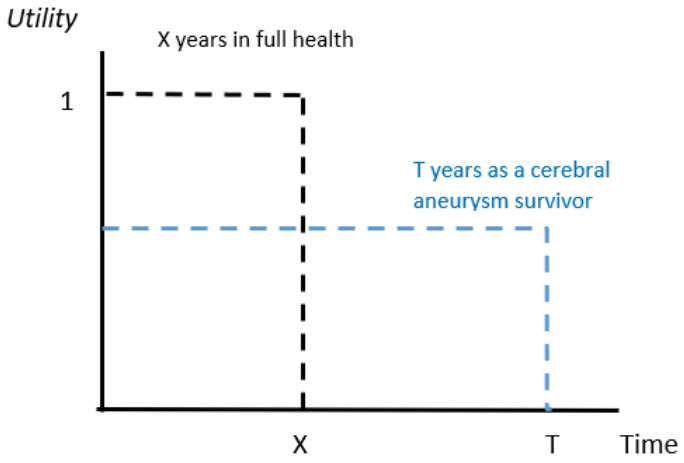

Figure 4.4: Time trade-off method.

In the Standard Gamble method, patient is asked to choose between a reduced state of health 'B' with a certain outcome of a life in illness or an immediate death and a gamble 'A' including a better clinical outcome and worse one such as death [28]. With a high probability of immediate death or severe disutility caused by the pathology, the subject will prefer the alternative 'A' and as the probability of surviving without treatment increases, the choice of gamble decreases to the point where the two will be indifferent to the subject [28]. The utility for a specific health state is given by the proportion between the two probabilities, that can be expressed as the risk that subject is willing to pay for improving own health related quality of life [28]. An example of Standard Gamble with object the problem of this study is shown in the *figure 4.5*. A patient with a cerebral aneurysm has to choose whether to undergo coiling endovascular therapy or not. The no-treatment (B) has as end results the immediate death or critical disabilities, while treatment (A) could improve the life condition by living in a specific mRS health state with a lower dying probability due to intra-procedural complications.

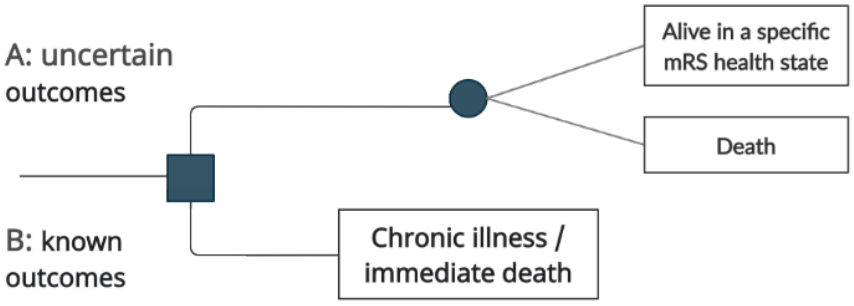

Figure 4.5: Standard Gamble method.

Quality of life measuring instruments of general validity have been developed and used mainly in the form of a questionnaire. The most used are:

- *36 Item Short-Form Survey (SF-36)*,
- *EuroQoL (EQ5D)*.

The SF-36 is used to quantify a general health condition and is structured in 36 questions that are divided into 8 domains: [26]

1. physical functioning;

2. discomfort due to physical problems;
3. bodily pain;
4. general health;
5. vitality;
6. social functioning;
7. psychological distress,
8. state of the mental health.

Patient can choose a score from 0 to 100 for each domain and higher scores reflect better outcomes [26]. The EQ5D instead is a questionnaire of 5 dimensions: [26]

1. mobility,
2. self-care,
3. usual activities,
4. pain or discomfort,
5. anxiety or depression

and questions of each dimension are quantified with three possible answers: no problem, moderate problem, or serious problem.

4.2.3 Perspective and Time horizon

In a pharmacoeconomic analysis the *perspective* must be predefined, that means from which point of view to calculate the costs [26]. The main perspectives that can be adopted are: [35]

- patient,
- society,
- hospital,
- health care system.

In an economic health analysis is necessary to set a *time horizon*, that is the period of time during which clinical outcomes and costs are taken into account [26]. It can be expressed as the patient's lifespan or the clinical follow-up time interval [26]. In the long-term analysis, the time horizon is several years, and the costs relating to the current year differ from those of previous years but also from the future costs, and for this reason a reference time period must be chosen with respect to which, all the costs examined must be reported [26]. The *discount rate* is applied to future values to express them according to the same time frame as current costs using the following formula:[26]

$$C_c = \frac{C_n}{(1+r)^n} \tag{4.2}$$

where C_c is the current cost, n is the number of future years, C_n is the future cost that will occur in n years and r is the discount rate [26].

4.3 Economic evaluation techniques

A health economic evaluation aims to compare costs and benefits related to more alternative treatments for a given clinical condition and there are different types of cost-outcomes analysis in which each differs from the others in the way of expressing the outcomes [26].

- *The cost-effectviness analysis* (CEA) allows to search for the therapeutic path for a given condition with the best cost-effectiveness ratio, that is the cheapest treatment parameterized to effectiveness [26]. The compared costs and outcomes of the several options are qualitatively identical but differ quantitatively [26]. The units of measurement of the results are natural unit e.g Life years saved (LYs), or reduction of the colesterol [26].
  If the new treatment A is more expensive but also more effective compared to the standard one B, the *incremental cost-effectiveness analysis* is more suitable because evaluates the incremental cost per unit of health gained through the *incremental cost-effectiveness ratio* (ICER), expressed as the ratio between the differences in average costs and average outcomes:[26]

$$ICER = \frac{C_A - C_B}{O_A - O_B} \tag{4.3}$$

  where C_n and O_n are the average costs and the average outcomes of the treatment n [26].

- *The cost-utility analysis* (CUA) has the same structure of the cost-effectiveness analysis but the outcomes are mesured in terms of QALYs [26]. This type of analysis consists in comparing the additional costs required by a treatment with the utility associated with the same [26]. The cost utility ratio is a useful parameter for comparing alternative strategies with different clinical results [26].

- *The cost-benefit analysis* is a type of economic evaluation in which both the costs and the benefits of the compared treatments are expressed in monetary terms and it is also useful in comparing strategies for different uses [26]. Outcomes are initially expressed in LYs or QALYs and subsequently translated into the corresponding monetary terms by adopting the *Willigness to pay* (WTP) criterion, which is the maximum expense that the health system is willing to pay [26]. The results can also be expressed as the *net monetary benefit* (NMB) obtained as the difference between the value of the benefits and the cost of obtaining them and a positive NMB values reflect the gain of the compared treatment [26].

- *The cost-minimization analysis* (CMA) is a variant of the cost-effectiveness analysis which is adopted in case of equivalent health outcomes of the compared alternative strategies and whose objective is to find which is the least expensive on the basis of the difference in health costs [26].

4.4 Study modeling process

4.4.1 Steps in Decision Analysis

The basic structure of the cost-effectiveness analysis is the *Decision Analysis* that is a systematic approach to make decisions in conditions of uncertainty represented by the two or more therapeutic strategies for a given clinical condition [26]. It consists of 4 steps:[26]

- identify the clinal problem and determine the possible treatments;
- structure the problem through the decision tree;
- identify clinical information for the compilation of the decision tree from clinical sources;
- choice of the best clinal path based on the outcomes found in the prior steps.

4.4.1.1 Identification and Definition of the decision problem

The first step of the decision analysis involves the identification of alternative pathways in front of a specific well-defined clinical problem. The example used, has as its object a patient with intracranial aneurysm / SAH undergoing coiling endovascular therapy. The possible clinical paths are differentiated by the type of cerebral coils used. The precise definition of the clinical problem and its alternative courses of action can be made on the basis of a previous literature review, as was done for this study. There are three macro categories of cerebral aneurysm coils available: *Bioactive coils*, *Bare Platinum coils*, and *Spectra Family coils* of which Spectra Bare Platinum coils are more interesting due to their reduced request for stents which could lead to a reduction in risk and costs. Endovascular treatment with Spectra Bare Platinum coils, has registered the use of additional medical devices of 29.4% of whom 9.8% are stents. The additional devices verified in the endovascular treatment with Bioactive coils are 41.88% of whom 12.90% are stents and 51.42% of whom 32.30% are stents in the endovascular treatment with Bare Platinum coils. The *table 4.1* shows in detail the additional medical devices values required during endovascular therapy with the three possible families of coils.

Table 4.1: Percentages of additional medical devices required during endovascular therapy

Family coils	**Device**	**Value %**
Spectra Bare Platinum	No added device	70.60%
	SAC	9.80%
	BAC	19.60%
	SAC+BAC	0.00%
Bioactive	No added device	58.12%
	SAC	12.90%
	BAC	24.10%
	SAC+BAC	4.88%
Bare Platinum	No added device	48.57%
	SAC	32.30%
	BAC	17.51%
	SAC+BAC	1.62%

Faced with this literature review, the two possible clinical paths to follow have been chosen: endovascular treatment with Spectra Bare Platinum coils (S-BP) or with Bioactive/Bare Platinum coils that represent the alternative strategy. The consequence of the chosen treatment, is the probability to have a good outcome in which the patient remains functionally independent, or a poor outcome resulting in a mild to severe disability due to a procedure complication, or the probability of death. At the end of the surgery a certain percentage of patients leaves the hospital with a good clinical results, another with mild or moderate-severe disability and another dies. In the current clinical condition, the short-term clinical outcomes were usually reported using the *modified Rankin Scale* (mRS). This scoring system measures the health condition of patients after hospital discharge, using 6 grades: mRS 0-2 reflects a good outcomes, mRS 3 indicates a mild disability, mRS 4-5 indicates a moderate to severe disability, mRS 6 is associated with death. This aspect has been included.

4.4.1.2 Creation of the decision tree

The second step is the creation of the decision tree which returns a visual and immediate description of the clinical problem highlighting three aspects: [35]

- the alternative therapeutic strategies that can be undertaken by the doctor;
- the events resulting from the choice;
- the clinical outcomes for the patient resulting from a possible treatment and related consequences.

The decision tree develops from left to right, and consists of a series of branches, a decision and chance nodes. A decision node drawn with a small square represents a point in time in which the doctor, when

faced with a given clinical problem, can choose among the possible therapeutic paths that branch off from the initial decision node [35]. Here, the decision is to treat a brain aneurysm / SAH patient using S-BP coils or alternative coils. To evaluate the most effective strategy, the patient is sent on both lines of action *(figure 4.6)*.

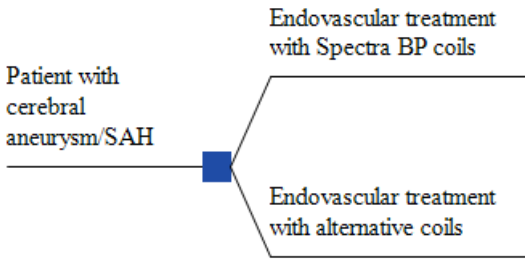

Figure 4.6: Partial Decision Tree with the initial decision node.

Probabilistic nodes (circular nodes) are added to each branch exiting the decision node to represent a point in time when uncertain events occur [35]. The clinical results resulting from the chosen treatment are uncertain and could be positive or negative. Each probabilistic branch ends in a terminal node represented with a triangle, that reflects the moment in time in which the outcomes identified above are reached. The decision tree describing the current clinical problem is now complete *(figure 4.7)*.

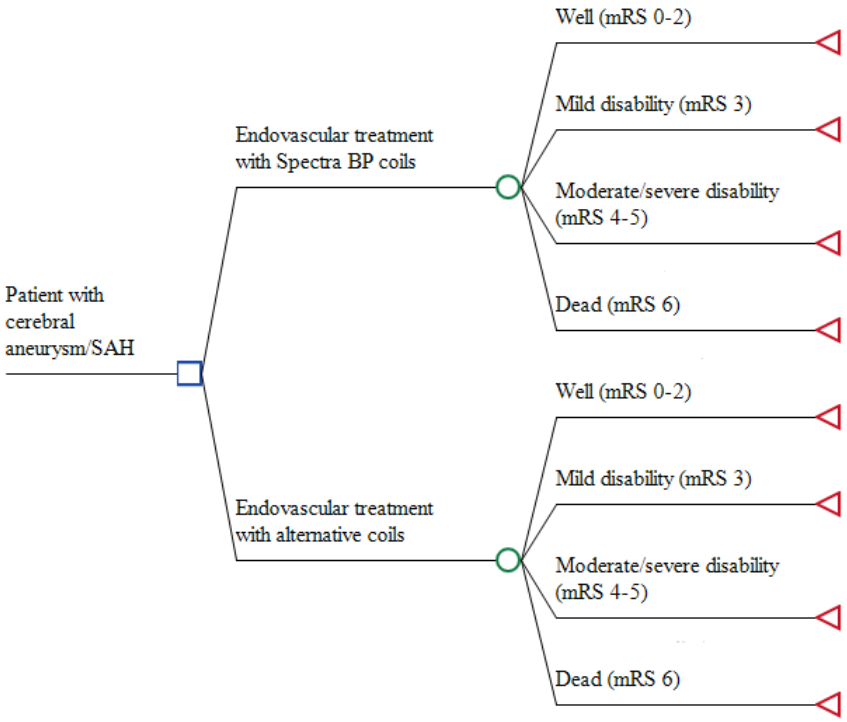

Figure 4.7: Complete Decision Tree used for the study.

4.4.1.3 Collection of clinical information

In the decision tree depicted in *figure 4.7*, a probability value is associated with each uncertain event as shown in *figure 4.8*. The probabilities are extracted from a clinical trials, clinical datasets, a prior scientific studies, a randomized controlled trials, a systematic review regarding safety and efficacy of a cerebral coils.

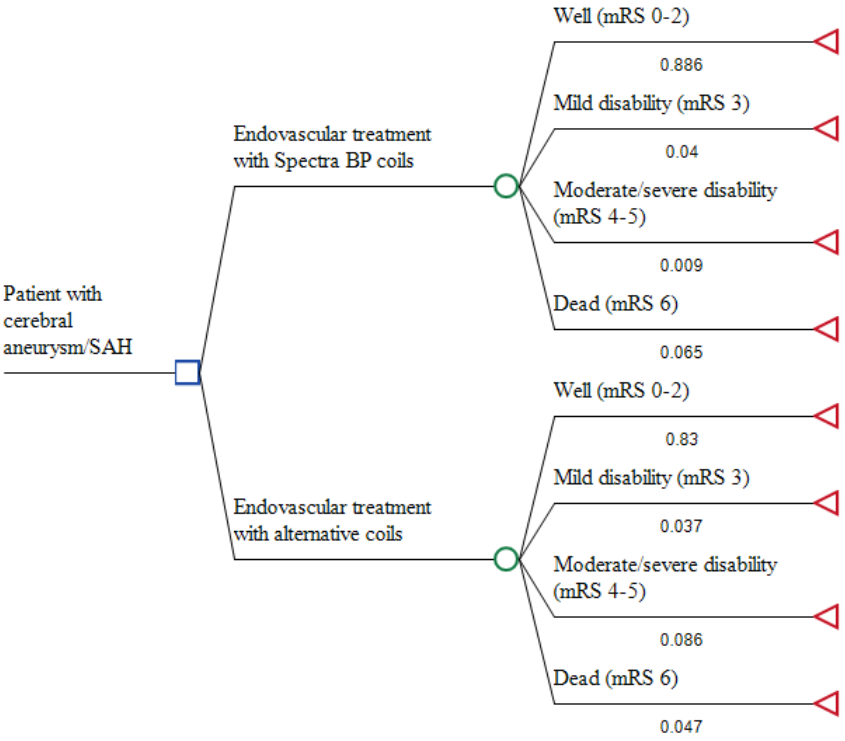

Figure 4.8: Complete Decision Tree used for the study with probabilities added.

4.4.2 Markov Model

Markov model is suitable for representing dynamic clinical problems that would require a very long time horizon and for this reason the effectiveness or the risk of a repeated event over time are quantified through a simulation of events [43]. It consists of a set of finite states N, called the *Markov states*, and transition probabilities between them [43]. The clinical condition of the patient is divided into a set of health states. The simulated patients are distributed according the vector of the initial population $P^{(0)}$:

$$P^{(0)} = \begin{bmatrix} p_1^{(0)} & p_2^{(0)} & \dots & p_N^{(0)} \end{bmatrix} \tag{4.4}$$

Each patient can transition from one state to another within a discrete time interval, called the *Markov cycle*, in which each simulated patient can only be in one of the states considered [43]. Each state is characterized by a set of transition probabilities that can be constant or time-dependent [43]. The expected values are calculated at the end of each cycle and sommed at the end of the simulation.
Markov model usually are incorporated into a decision analysis tree, because recycling of a specific condition may be repeated, and is therefore much easier to represent. Markov model allows to simulate more complex consequences of an option. Markov model has some limitations in representing a real clinical condition, since all the patients of the simulated cohort occupy a single state at the same time [28]. In addition, Markov models are said to be memoryless as the possible transitions from one state to another that individuals can make depend only on the state they are in and not on their previous path [43]. This is the main limitation of the model in describing clinical pathways, where probable events may occur following a verified event.

4.5 Sensitivity Analyses

The nature of the large amount of data relating to the parameters of a pharmacoeconomic model is deterministic, since the sources are characterized by their own level of uncertainty [35]. These uncertainties are related to the estimated values of some unavailable data or to the available data affected by inaccurate assessments or to the method used in the evaluation and it is important to determine the effect on the results due to the variability of the parameters in the range of their possible values [35]. Uncertainty can be defined as the error related to the value of a data, different from the concept of variability which measures how a characteristic varies within the simulated population. Data are generally expressed through a point estimate i.e a mean and 95% confidence interval taken into account [26]. Conducting a *sensitivity analysis* is the way to assess uncertainty in a pharmacoeconomic study [26]. A sensitivity analysis is developed in three phases: [35]

- identification of uncertain data,
- definition of the range of probable values,
- calculation of the results along these ranges.

To decide which data are affected by uncertainty, it is necessary to understand their origin: the age and sex of the simulated cohort are certainly average values, therefore affected by uncertainty, instead, the costs of a given drug or hospital costs according to the DRG tariffs tend to be fixed and could be excluded. The minimum and maximum of the range of possible values could be established by reviewing the available scientific literature.
The sensitivity analysis can be deterministic (*Deterministic Sensitivity Analysis, DSA*) and probabilistic (*Probabilistic Sensitivity Analysis, PSA*), both are intended to investigate the uncertainty of the results of a model, and are highly recommended by the ISPOR (*International Society for Pharmacoeconomics and Outcomes Research*) guidelines [44].
There are four different approaches used in a DSA: [35]

- One-way sensitivity analysis,
- Multi-way sensitivity analysis,
- Threshold analysis,
- Extreme case (worst- and best-case scenario) analysis.

One-way sensitivity analysis is the simplest method, in which the input values for a parameter are varied one at a time in their range of probable values, keeping the base values for all others to highlight how the results will change, while in *multi-way analysis*, the effects on the results of the simultaneous variation of two or more inputs values at the same time are evaluated [35].
In the *threshold analysis*, which is a variant of the one-way analysis, the value of a variable is varied in order to find a threshold value above or below which the results are not accepted or require a particular intervention [35].
Finally, in *extreme case analysis*, as the name suggests, worst and best scenarios are analyzed through a multi-way analysis based on a combination of the worst or best values of the model inputs [35].
The results of deterministic sensitivity analysis are usually represented by *tornado diagrams*, a bar charts which provide a representation of the overall variation of the model result with the vary of each input parameters between the extreme values of the respective range, and graphically each bar represents variation range for each of the considered parameters positioned vertically in descending order of sensitivity, in order to highlight those that have the largest variation and therefore that most influence the final results [26].
Probabilistic sensitivity analysis (PSA) is a technique used in economic modeling to quantify the impact of uncertainty in model inputs on the results of the analysis [43]. In PSA the input variables are varied simultaneously, sampling them from specific probability distributions based on the 95% confidence interval or the standard error, derived from meta-analysis or clinical studies [43]. Different distributions are generally appropriate for different types of variables such as risks, hazard ratios and costs can be sampled from a Lognormal distribution which always returns positive values [43]. PSA involves repeating

the Markov model many times (generally 10,000), in each of which all the parameters used in the base case will be different as they are sampled directly or indirectly from an appropriate distribution. The results will be a joint-distribution of the outputs (costs and benefits) that can be represented by a scatterplot in the *cost-effectiveness plane* (CE): the incremental costs and benefits are reported on the ordinate axis and on the abscissa axis respectively and the final results form a cloud of points on the CE plane around the expected value of the base case [43]. The cloud gives a visual information about the stability of the model and the more compact it is, the lower the variability of the model, and consequently the more reliable the result [43]. One way to visualize the uncertainty of the expected value is to add the 95% confidence ellipse to the CE plane which delimits the area where the results fall with a 95% probability. Four quadrants can be identified in the CE plane as can be seen in *figure 4.9*. If the new strategy saves money and improves health, it dominates the competitor, while if it requires incremental costs and worsens health, it is said to be dominated by the competitor. If the cloud of results is in the cost increase and effectiveness improvement quadrant, the *willingness to pay* (WTP) by the payer should be assessed. Thresholds need to be defined. NICE (National Institute for Clinical Excellence) defines a cost-effective strategy at maximum acceptable ICERs of £20,000–£30,000 per QALY gained[69]. However new drugs for rare diseases can be evaluated using higher thresholds.

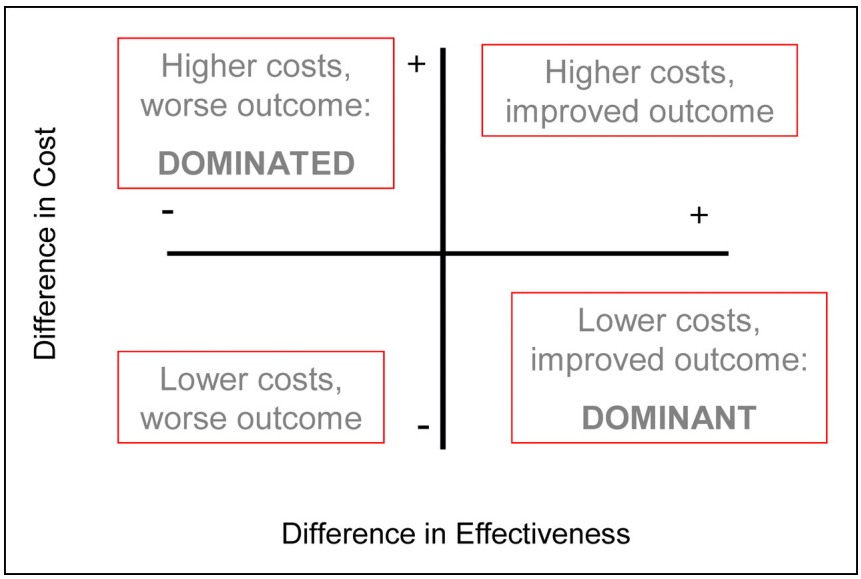

Figure 4.9: The cost-effectiveness plane [71].

The results of PSA can be represented in an alternative way using a *cost-effectiveness acceptability curve* (CEAC) that plots the hypothetical WTP per unit of benefit earned on the x-axis (the cost-effectiveness threshold considered acceptable by the payer) and the probability that a treatment is cost-effective compared with the alternative, on the y-axis [43]. The CEAC gives a visual indication of the percentage of PSA results that give a lower cost-effectiveness than a specific WTP and for a given maximum WTP, the probability that the intervention under assessment is cost-effective or not compared with the alternative is read in correspondence [43]. The uncertainty associated with the decision to introduce the treatment or not is given by the inverse of this probability (1-probability) [43]. Therefore, the CEAC helps the decision maker to better understand the impact of uncertainty on the outcome of an intervention, in relation to the possible values of the cost-effectiveness threshold.
PSA can be conducted both within a patient-level model and within a cohort-level model. Cohort-level simulation is a type of modeling in which at each cycle of the simulation, the behavior of the population is an average behavior. The components of the hypothetical cohort are simulated as if they all had the same characteristics. In microsimulation there is a cohort where each component that can be a patient has its own behavior / characteristics and each is simulated individually. For example, there is no average age, but an age is associated with each subject, sampling it from an appropriate distribution characterized by mean value and standard deviation which constitute the parameters to be sampled in the PSA. The great difference of the PSA conducted at the patient level is that it also allows to investigate the variability of

the hypothetical cohort, simulating a condition much closer to the real one.

4.6 Case study: Endovascular Coiling Treatment of Cerebral Aneurysm

A cost-utility analysis was conducted to compare endovascular coiling with S-BP coils versus endovascular coiling with alternative coils in patients with cerebral aneurysm or SAH.

4.6.1 Model Structure

A two-step model was built in Microsoft Excel 2016 to assess the cost-utility of the two compared strategies. It was assumed that all aneurysms were discovered before patients arrived at the hospital, so the screening procedure was not included in the first hospital phase. The in-hospital pathway of each patient undergoing coiling with S-BP or coiling with alternative coils was simulated using a decision tree (*figure 4.7*). Each iteration of the simulation represents the same patient who is sent simultaneously on both action lines of the model (S-BP vs alternative coils). Treatment of aneurysms may have a short-term risk of procedural complications that lead to poor outcomes such as mild or moderate-to-severe disability and in the worst case, death. Even for surviving patients there may be a recurrence of the aneurysm with the need for retreatment during the remaining life. After hospital discharge, a Markov model *(figure 4.10)*, with annual cycles, was used to simulate the effect of risk on a patient's life expectancy given the different concurrent mortality risks related to age, disability and eventual retreatment. The clinical outputs of the in-hospital phase were used as starting point into the Markov model. The model simulates a hypothetical cohort of patients until the death of all, and each can be in one of four health states:

- alive in a disability state without a recurrence of aneurysm/SAH;
- retreatment;
- alive post-retreatment in the same or higher level of disability;
- dead.

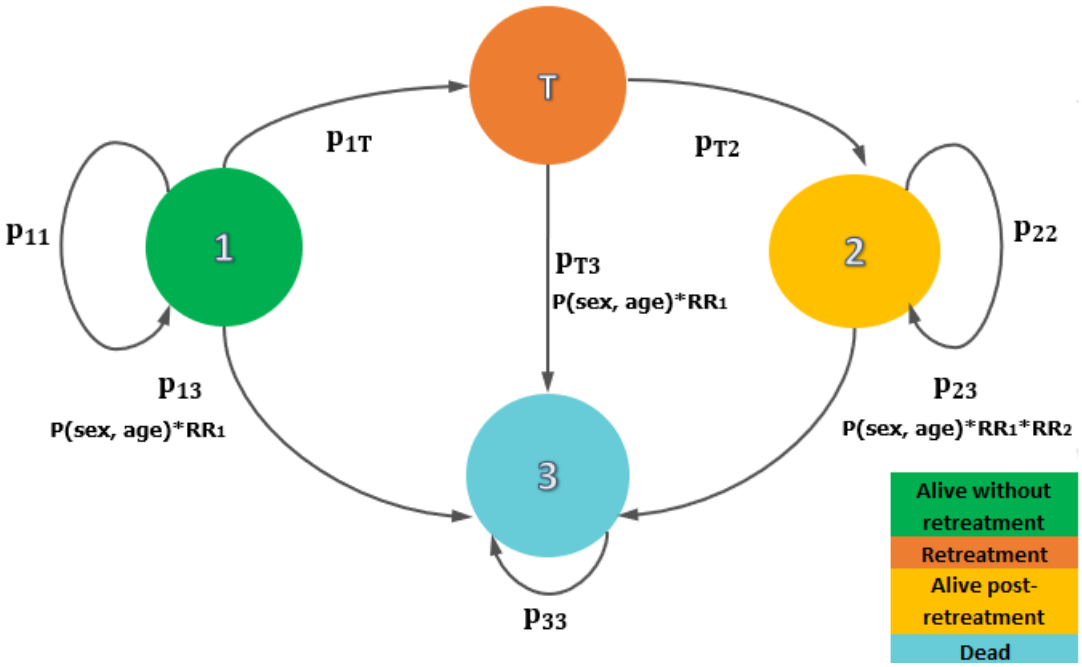

Figure 4.10: Markov Model diagram. The circle labeled "T" represents a tunnel state.

The state labeled "retreatment" is a tunnel state that represents an event with short-term effects. The brain aneurysm may recur with the need for retreatment and the patient can spend no more than a single cycle on this state. It was hypothesized that the patient could be re-treated only one more time due to the high risk of the operation.
Transition probabilities used in the Markov model depend on the disability level after hospital discharge. In this study a health care system perspective is adopted for evaluating costs. A 3.5% annual discount rate was applied to both costs and outcomes.

4.6.2 Model Inputs

The model inputs were derived from the sistematic review conducted during this thesis work. The base value of the inputs is based on data of the most recent meta-analysis, prospective and cohort studies conducted from 2003 to 2019.

4.6.2.1 Hospital exitus and Transition Probabilities

The short-term clinical outcomes have been reported using the *modified Rankin Scale* (mRS). Hospital exitus with specific mRS health state was assumed age-independent and derived from hospital outcomes collected in the sistematic review.
The transition probabilities consisted of the probability of remain in a specific mRS health state, the annual aneurysm retreatment probability, the probability of annual death, including that as a result of retreated aneurysm. The probability of retreatment was assumed to be age-independent. The annual death probability was expressed as a function of sex and age based on the US life table for the male and female population reported in *Appendix B* [27]. This probability was obtained as the weighted average between the mortality of men and the mortality of women according to the total probability theorem and at each iteration these two probabilities were updated based on the data of the US life table. The mortality rate without a retreatment event was age and sex adjusted hazard ratio (HR) associated to each mRS health condition [30]. The probability of death associated with a retreatment event is higher due to the high procedural risk, therefore the risk of death from a given disability level related to the procedure was included. The probability of post-retreatment death was further improved with the risk of post-retreatment mortality in men and women [29].
Model probabilities and patient characteristics are detailed in *table 4.2*.

4.6.2.2 Utilities

Each therapy effectiveness was measured using the QALYs, calculated by multiplying years spent in a specific mRS health state by the utility weight for that health state. Utility weights were derived from a recent survey [31]. Utilities values were considered age-indipendent, in line with several studies on health-related quality of life after cerebral aneurysm, which stated that the patient's age does not affect utility weights. Utility values are between 0 correlated to the death and 1 reflecting a good health, and generally decrease with a greater disability. Utilities for mRS health state are listed in *table 4.3*.

4.6.2.3 Costs

Costs considered in the analysis are direct health care costs. Both direct in-hospital and long-term costs were analyzed (*table 4.4*). The in-hospital costs for each therapeutic procedure include overall hospitalization costs from hospital stay and diagnostic exams to operating room including cost for the different type of device used (coiling alone, additional device such as stent, ballon or stent plus ballon). Long-term costs were stratified for each mRS health states following the intervention and derived from a recent costs study [40]. It has been assumed that mRS 0-2 health condition has no long-term annual costs as the patient is discharged with good clinical outcomes. In addition to the long-term costs, there is the post-treatment cost of antiplatelet therapy (APT) which is only given to stented-patients. Costs of retreatment were assumed to be 85.6% of hospital costs.

Table 4.2: Model probabilities and patient characteristics.

Parameters	Base Case	Range	Reference
Baseline characteristics			
Age (yrs)	54.68	51 – 58	Sistematic Revision
% Sex female	66.46%	60.90 – 80.00%	Sistematic Revision
Short-term outcomes			
% No added device S-BP	70.60%	70.60 – 70.60%	Sistematic Revision
% Added stent S-BP	9.80%	9.80 – 9.80%	Sistematic Revision
% Added ballon S-BP	19.60%	19.60 – 19.60%	Sistematic Revision
% Added stent+ballon S-BP	0.00%	0.00 – 0.00%	Sistematic Revision
%No added device other coils	51.10%	48.60 – 58.10%	Sistematic Revision
% Added stent other coils	27.20%	12.90 – 32.30%	Sistematic Revision
% Added ballon other coils	19.20%	17.50 – 24.10%	Sistematic Revision
% Added stent+ballon other coils	2.50%	1.60 – 4.90%	Sistematic Revision
%Well (mRS 0-2) S-BP	88.58%	78.95 – 93.10%	Sistematic Revision
%Mild disability (mRS 3) S-BP	4.00%	2 – 8.27%	Sistematic Revision
%Moderate/severe disability (mRS 4-5) S-BP	0.96%	0 – 3%	Sistematic Revision
%Dead (mRS 6) S-BP	6.46%	4.90 – 9.78%	Sistematic Revision
%Well (mRS 0-2) other coils	83.05%	66 – 97.80%	Sistematic Revision
%Mild disability (mRS 3) other coils	3.70%	0 – 15%	Sistematic Revision
%Moderate/severe disability (mRS 4-5) other coils	8.60%	0 – 20.30%	Sistematic Revision
%Dead (mRS 6) other coils	4.65%	0 – 19.20%	Sistematic Revision
Long-term outcomes			
%Retreatment S-BP coils	5.90%	5.10 – 9.70%	[37], [38], [39]
%Retreatment other coils	8.20%	8 – 8.80%	[37], [38], [39]
Risks			
Procedure mortality rate S-BP coils	0.5%	0 – 1.4%	Sistematic Revision
Procedure mortality rate other coils	1.53	0.90 – 1.90%	Sistematic Revision
Post-retreatment mortality ratio Men	11.45	7.42 – 15.48	[29]
Post-retreatment mortality ratio Women	18.93	8.22 – 29.64	[29]
Death hazard rate ratio mRS 0-2	1	0.82 – 1.56	[30]
Death hazard rate ratio mRS 3	1.66	1.24 – 2.23	[30]

Table 4.3: Utilitis for mRS health state.

Baseline Utility	Base Case	Range	Reference
Good outcomes (mRS 0-2)	0.91	$0.87 - 0.94$	[31]
Mild disability (mRS 3)	0.76	$0.65 - 0.84$	[31]
Moderate/severe disability (mRS 4-5)	0.25	$0.16 - 0.37$	[31]
Death (mRS 6)	0	$0 - 0$	[31]

Table 4.4: Costs Inputs

Cost	Base Case	Range	Reference
In-hospital costs			
Coiling alone procedure	$\$16,300$	$7,339 - 56,958\$$	[42]
SAC procedure	$\$28,413$	$5,190 - 82,017\$$	[42]
BAC additional cost	$\$1,000$	$800 - 1,200\$$	[70]
Long-term costs			
Annual cost mild disability	$\$1,163$	$930 - 1,396\$$	[40]
Annual cost moderate/severe disability	$\$25,686$	$20,549 - 30,824\$$	[40]
Annual cost antiplatelet therapy	$\$1,093$	$857 - 1,396\$$	[41]

4.6.3 Cost-Utility Analysis

The two strategies were compared in terms of incremental costs and incremental effectiveness. The base-case analysis represents the cost-utility analysis using the base value of the all model inputs. The 1-way deterministic sensitivity analysis (DSA) is performed to investigate the effect of the single parameters variation on the outcomes. In the DSA, all parameters were varied one by one, taking the maximum and minimum of the observed interval. The results have been represented using a tornado diagram. In addition, a probabilistic sensitivity analysis (PSA) was conducted to investigate the impact of uncertainties about input parameters on the results. PSA simulation was performed with 1,000 iterations, modeling 1,000 cohorts of patients, sampling all model parameters (except age and discount rate) from appropriate distributions (see *table 4.7*). The analysis results have been shown in the incremental cost-effectiveness plane with the 95% confidence ellipse added. Cost-effectiveness acceptability curve (CEAC) was adopted to quantify and graphically represent uncertainty of S-BP coiling to be cost-effective.

4.7 Results

4.7.1 Base-Case Analysis

The base-case scenario demostrated that S-BP coiling has lower costs and higher effectiveness, making it the dominant strategy (*Tables 4.5, 4.6*). Retreatment in S-BP coiling is lower than that of endovascular therapy with alternative coils (2.10% vs 2.40%), with also an improvement in the lifetime survival (12.43 vs 11.81 life years). SB-P coiling provides more QALYs over a lifetime with a mean gain of 1.15 QALYs. Mean hospital saving due to SB-P coiling is \$2,432, while the long-term costs of endovascular treatment with alternative coils are much higher than those for S-BP (\$60,932 vs \$30,697) requiring an incremental total cost of \$30,235.

Table 4.5: Effectiveness results: values expressed as mean

	S-BP coils (st1)	**Alternative coils (st2)**	**Delta (st1 vs st2)**
Life Years	12.43	11.81	+0.62
Retreatment	2.10%	2.40%	-0.30%
QALY	11.16	10.01	+1.15

Table 4.6: Economic results: values expressed as mean

	S-BP coils (st1)	**Alternative coils (st2)**	**Delta (st1 vs st2)**
In-hospital costs	$17,683	$20,115	−$2,432
Long-term costs	$13,014	$40,818	−$27,804
Total costs	$30,697	$60,932	−$30,235

Figures 4.11 and *4.12* provide a general indication of the probability of transition in the three health states of the hypothetical simulated cohort if subjected to S-BP coiling and endovascular treatment with alternative coils, respectively. As can be seen, patients discharged alive after S-BP coiling experience fewer reoperations than those subjected to coiling with alternative coils, with an analogous lengthening in the lifetime survival.

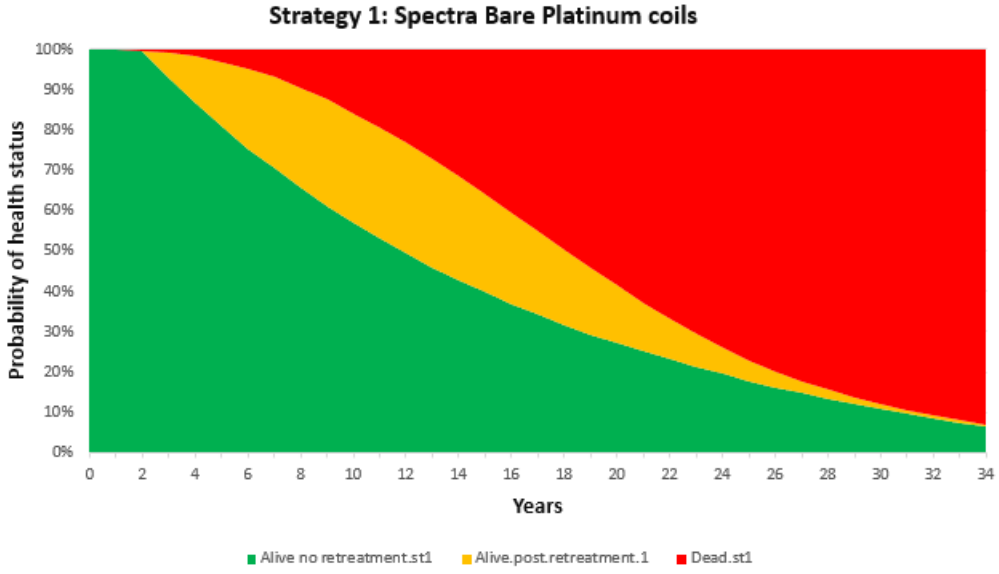

Figure 4.11: Transition probability of health status in endovascular treatment with S-BP coils.

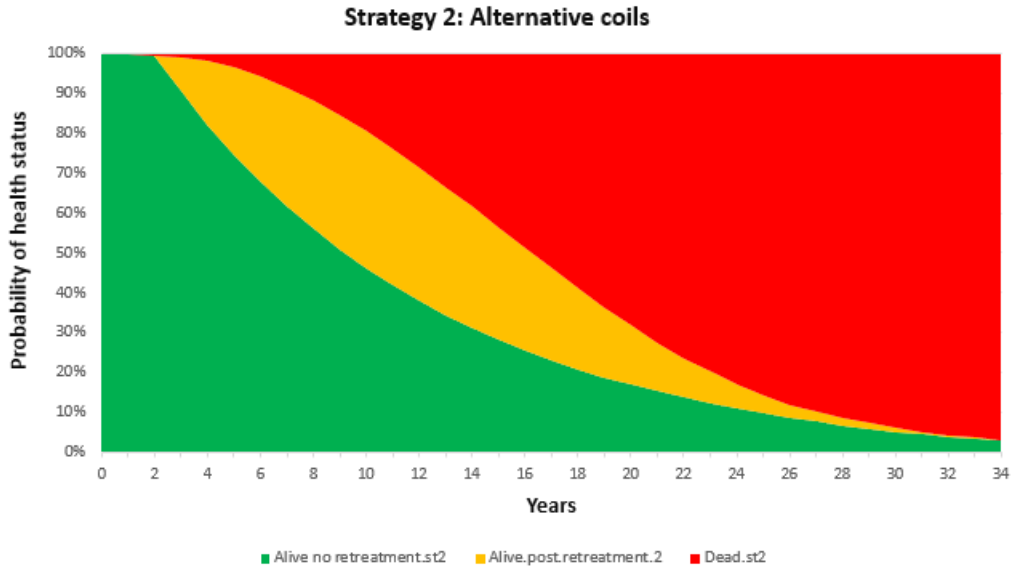

Figure 4.12: Transition probability of health status in endovascular treatment with alternative coils.

4.7.2 Deterministic One-Way Sensitivity Analysis

In *Figures 4.13 and 4.14* are reported the deterministic sensitivity analysis results. The base-case values are -$30,235 savings and +1.15 gains. One-way sensitivity analysis in terms of savings demonstrated that for all parameters except the percentages of moderate to severe disability in the 2^{nd} strategy, the results are in line with the base case. Furthermore, although the total saving is very sensitive to this parameter, even for more conservative values, the S-BP strategy remains the most economical strategy (Min= -$25,694). One-way sensitivity analysis in terms of earnings showed that the cost-utility analysis is more sensitive to changes in the percentages of the disability level and the retreatment rate. As the number of patients with good outcomes in the competitor increases, the gains decrease (Min=-0,53 QALYs), the same picture is confirmed with the increase in the retreatment rate of S-BP coiling (Min=-0,02 QALYs).

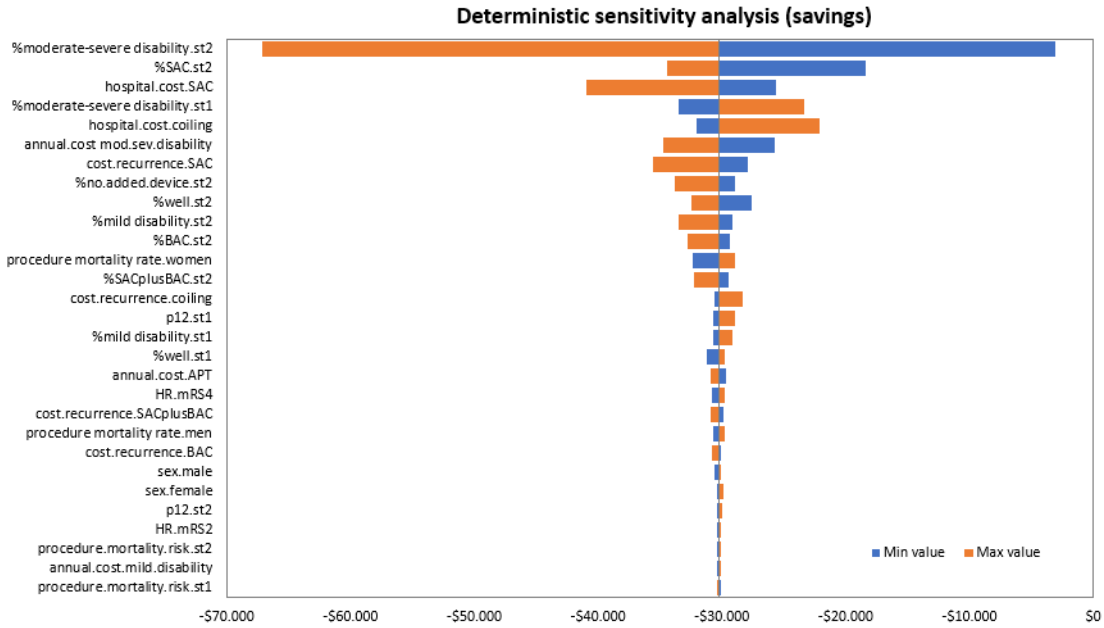

Figure 4.13: Tornado diagram depicting 1-way sensitivity analysis in terms of savings.

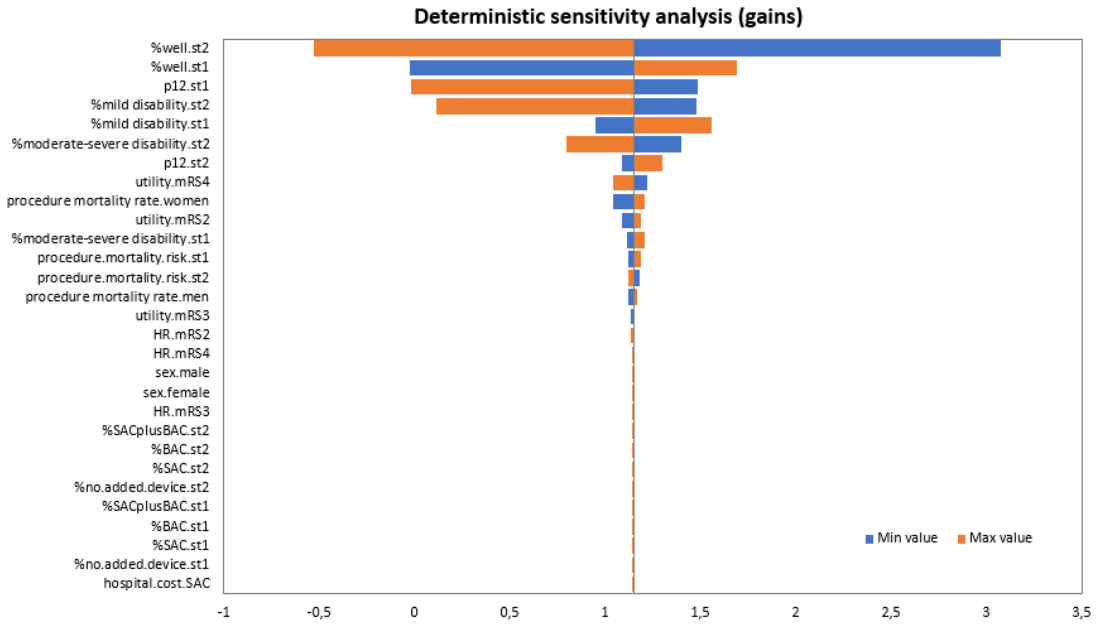

Figure 4.14: Tornado diagram depicting 1-way sensitivity analysis in terms of gains.

4.7.3 Probabilistic Sensitivity Analysis

The PSA results (*Figure 4.15*) confirm that S-BP coiling is the most cost-effective strategy, with a 95% confidence ellipse lying almost completely in the dominant area of the cost-effectiveness plane. Cost-effectiveness acceptability curve with different WTP thresholds are shown in *Figure 4.16*. The S-BP coiling versus the competitor has an estimated 95% probability of being cost-effective even when the decision maker is willing to pay up to 300,000$/QALY. The CEAC cuts the y-axis at 1, because the entire density involves savings in cost. The CEAC asymptotes to a value less than 1, because the S-BP coiling does not provide health gains and cost-savings in all cases (1.7%).

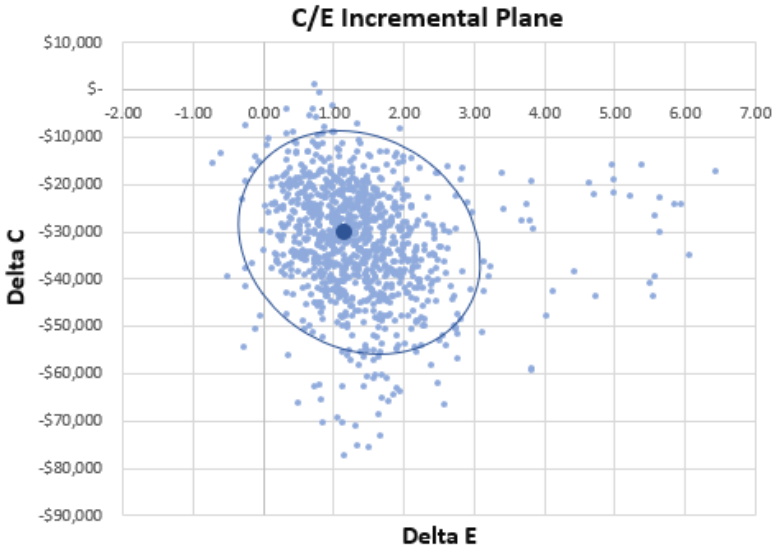

Figure 4.15: Incremental cost-effectiveness plane scatterplot.

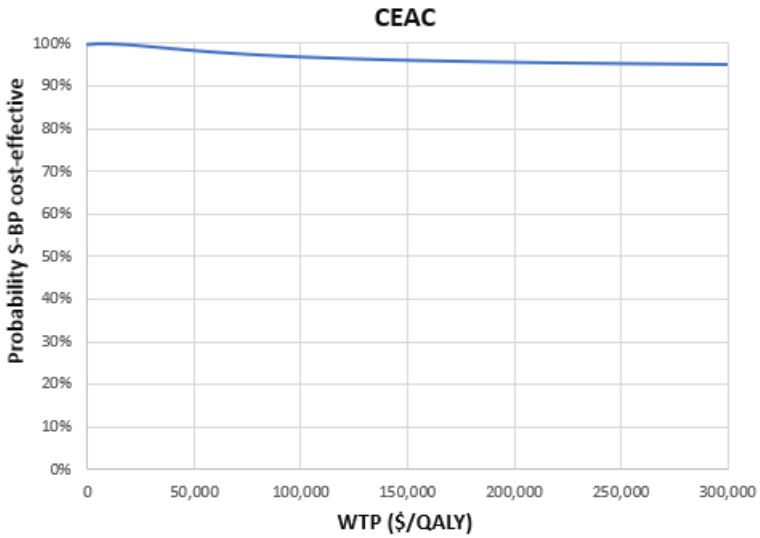

Figure 4.16: Cost-effectiveness acceptability curve.

Table 4.7: Model Inputs investigated in the PSA

Model Input	**Distribution**	**Mean (SE)**
% Sex female	normal*	0.667(0.02)
%Well (mRS 0-2) S-BP	dirichlet	0.865(87.12)
%Mild disability (mRS 3) S-BP		0.075(7.52)
%Moderate/severe disability (mRS 4-5) S-BP		0.0053(0.54)
%Dead (mRS 6) S-BP		0.055(5.5)
%Well (mRS 0-2) other coils	dirichlet	0.81(82.88)
%Mild disability (mRS 3) other coils		0.23(2.44)
%Moderate/severe disability (mRS 4-5) other coils		0.11(10.86)
%Dead (mRS 6) other coils		0.06(6.25)
% No added device S-BP	dirichlet	0.64(65.69)
% Added stent S-BP		0.107(11.07)
% Added ballon S-BP		0.253(26.02)
% Added stent+ballon S-BP		0(0)
%No added device other coils	dirichlet	0.573(55.42)
% Added stent other coils		0.273(26.36)
% added ballon other coils		0.125(12.09)
% Added stent+ballon other coils		0.03(2.81)
%Retreatment S-BP coils	normal*	0.081(0.18)
%Retreatment other coils	normal*	0.082(0.03)
Procedure mortality rate S-BP coils	normal	0.0178(2.44)
Procedure mortality rate other coils	normal	0.0123(0.19)
Post-retreatment mortality ratio Men	normal	8.36(0.19)
Post-retreatment mortality ratio Women	normal	22.5(0.33)
Death hazard rate ratio mRS 0-2	normal	1.1(0.16)
Death hazard rate ratio mRS 3	normal	2.15(0.15)
Death hazard rate ratio mRS 4-5	normal	2.15(0.16)
Utility Good outcomes (mRS 0-2)	normal*	0.92(0.21)
Utility Mild disability (mRS 3)	normal*	0.76(0.27)
Utility Moderate/severe disability (mRS 4-5)	normal*	0.22(0.28)
Coiling alone cost	normal	13,049(0.52)
SAC cost	normal	32,554.3(0.70)
BAC additional cost	normal	1,018.4(0.10)
Annual cost mild disability	normal	1,203.79(0.10)
Annual cost moderate/severe disability	normal	29,595.9(0.10)
Annual cost antiplatelet therapy	normal	1,132(0.12)

*To limit the value of the sample value p between 0 and 1, the logit of p was sampled.

4.8 Discussion

The ascertained prevalence of the minimally invasive technique of coiling alone in the treatment of ruptured and unruptured cerebral aneurysms, and the high variety of coils available, stimulate the interest of decision maker and of patients to know more about the cost-effectiveness of this treatment using different families of coils. Whereas previous cost-effectiveness studies evaluated surgical treatment versus coiling alone or versus SAC for the treatment of cerebral aneurysms/SAH, the current study is the first to examine the cost-utility of endovascular coiling treatment with different families of coils.
In this cost-utility analysis, coiling with S-BP coils is compared to coiling with alternative coils.
SB-P coiling was more cost-effective than coiling with alternative coils yielding 1.15 QALYs and $30,235 savings. The model is mainly influenced by changes in the hospital cost of SAC. Frontera et al. (2012, [42]) reported a large variance in the SAC costs ($5,190 - $82,017) and endovascular coiling ($7,339 - $56,958). Moreover, probabilistic sensitivity analysis stated that S-BP coiling has a 95% probability of being cost-effective even when decision maker is willing to pay a maximum threshold of $300,000/QALY and it has been confirmed to be the dominant strategy in 98.3% of 1,000 simulated cohort iterations, in comparison with coiling using alternative coils.
This model has several limitations. Short-term data refer to general treatment, without clinical outcomes distinction in the added devices or no added. This is due to the lack of data on clinical outcomes specific for these subcases. For the same reason, utilities with lower weights were not associated in the year in which the patients were subjected to retreatment.
The model does not include the distinction between narrow-necked and wide-necked aneurysms which certainly affects the total endovascular coiling costs and the recurrence rate which is less frequent in wide neck aneurysms treated with stents. Nishido et al. is reported that although SAC is associated with a reduction in the recurrence rate relative to coiling, on the other hand there is a higher procedural complication rate resulting in higher mortality [73]. The increase in ischemic events reported in stent-coiled patients compared to coiled one may be due to the major risk factors associated with the characteristics of the aneurysm and post-procedure antiplatelet therapy [72]. Future cost-effectiveness study comparing endovascular techniques may investigate the impact of short and long-term complications after each subtype.
The main limitation consists in the lack of price lists for specific coils by producer (S-BP coils and alternative coils). In reality, this study has the main purpose of providing a relative comparison of the initial general costs associated with the use of S-BP coils compared with those of all other coils and how the reduction in stent request associated with their particular structure impacts on costs, rather than accurately determining the cost of embolization procedures with the different coils.

Chapter 5

Conclusions

In the present work, the models of a middle cerebral artery with an untreated and treated aneurysm were employed to study the impact of two different rheological models of blood on hemodynamic parameters and the effects induced by the endovascular coiling technique. The interaction of blood with the aneurysm wall was performed with a Newtonian and non-Newtonian models. Even if the results do not show a significant differences between the two models, the Newtonian model overestimates the haemodynamic parameters and consequently leads to an underestimation of the rupture risk of anuerysm. It has been shown how the endovascular coiling method can be proposed as a valid treatment for cerebral aneurysm occlusion. The FSI technique is confirmed to be a powerful method to accurately predict the clinical outcomes of endovascular coiling treatment, taking into account the non-Newtonian effects of the blood and the hyperelastic behavior of the artery walls.
In addition, the cost-effectiveness analysis has shown that the endovascular coiling treatment is, in particular, more cost-effective using S-BP coils than all the other coils available commercially. Patients undergoing S-BP coiling compared to those undergoing alternative coils showed improvements in both survival and quality of life.

Chapter 6

Future Developments

In this work a finite element method has been developed to simulate the hemodynamic changes due to the endovascular coiling technique for the treatment of cerebral aneurysm. Obviously, the model incorporates simplifying assumptions, starting from the ideal geometry used. To improve the accuracy of the current study, many future steps could be developed.
A future development will be to investigate better hemodynamics with the distribution of the coils as the type of coil family varies, Spectra Bare Platinum and the other coils, using the same method used in the current study, FEM and FSI analysis. To evaluate the velocity reduction and coil distribution in aneurysms, new parameters will be adopted.
The *volume embolization ratio* (VER) defined as the ratio of inserted coil volume to aneurysm volume: [75] [76]

$$VER = \frac{Coil\ volume}{Aneurismal\ volume} \tag{6.1}$$

This parameter is also known as packing density, used in the clinical studies to evaluate the coil deployment that has been related to aneurysmal occlusion [77].
Parameter that focuses on the inflow neck area is the *neck volume embolization ratio* (NVER), defined as follows: [75] [76]

$$NVER = \frac{Coil\ volume\ in\ neck}{Neck\ inflow\ volume} \tag{6.2}$$

in which the inflow neck volume coincides with the volume of the region with blood velocity greater than zero in the Z direction in the neck and the coil volume neck is the volume of coils located in the neck inflow volume.
The *velocity reduction rate* (VRR) and the *wall shear stress reduction rate* (WSSRR) will be used to quantify hemodynamic changes after coiling embolization, defined as follows:

$$VRR = 1 - \frac{Averaged\ Velocity\ in\ aneurysm_{after}}{Averaged\ Velocity\ in\ aneurysm_{before}} \tag{6.3}$$

$$WSSRR = 1 - \frac{Averaged\ WSS\ in\ aneurysm_{after}}{Averaged\ WSS\ in\ aneurysm_{before}} \tag{6.4}$$

The two models of coils (Spectra Bare Platinum and at least one of the alternative coils) will be made on the basis of the characteristics of the real cerebral coils available on the market, while the aneurysm model used in this study will be maintained. The coils are formed from a wire of composition 92% platinum and 8% tungsten alloy, wound in a first helical structure, and the whole coil is wound to form a secondary helical spring structure, which will be modeled as mathematical curve generated from parametric equations derived by Babiker et al. [74]. In this way the shape memory of the cerebral coil will be taken into account, which means that the coil is able to recover its pre-shape during its deployment inside the aneurysm sac, thanks to the deformation energy stored during advancement into the catheter.
The best way to simulate the coil packaging, the coil advancement and the coil deployment is to use

the Abaqus software. The deployment of the coil from the catheter will be simulated. As boundary conditions for the movement of the coil, the same conditions in Babiker et al. [74] can be used, which impose a sliding of the coil with a speed of 10 mms^{-1} inside the catheter and a release in the aneurysm at 5 mms^{-1}, as soon as the distal tip of the coil reaches that of the catheter positioned in the center of the aneurysm. For coil-to-coil, coil-aneurysm and coil-to-catheter interaction, coefficients of friction should be considered. Once the coil has been unfolded, it will be possible to perform the second future step, the FSI analysis with the same boundary conditions of this study. In the end, it will be possible to compare the estimated packing density results with the values reported in clinical studies.

Appendix A

Hyperelastic material

Many studies have shown how the mechanical properties of the brain aneurysm are best described by a model of hyperelastic incompressible material. The hyperelastic material models available are the following:

- Neo-Hookean,
- Fung,
- Mooney-Rivlin two parameters,
- Mooney-Rivlin five parameters,
- Ogden,
- Polinomial,
- Saint Venant-Kirchhoff,
- Yeoh,
- Blatz-Ko,
- Extended Tube.

The Mooney-Rivlin five parameters model was stated the most accurate. In this study the Mooney-Rivlin two parameters model has been used for describing the aneurismal sac properties and the Neo-Hookean model for describing the arterial mechanics. The choices were made to reduce the several iterations required by the Mooney-Rivlin five parameters model and therefore, a longer calculation time.

A.1 Local Deformation

Let P be a material point with position X occupied in initial non-deformated configuration and the x position occupied as a result of deformation (see *figure A.1*).

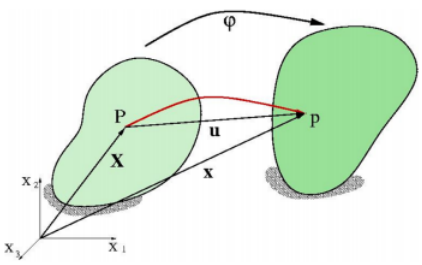

Figure A.1: Kinematics of a material point.

Local change from initial configuration to the current one is described by the deformation gradient F:

$$F = \frac{\partial x}{\partial X} \tag{A.1}$$

The determinant of F is always positive and is defined as follows: [57]

$$J = detF > 0 \tag{A.2}$$

Starting from the deformation gradient, the Cauchy-Green strain tensor can be expressed as: [57]

$$B = F^T F \tag{A.3}$$

whose invariants are:

$$I_1 = tr(B) \qquad I_2 = \frac{1}{2}[(tr(B))^2 - tr(B^2)] \qquad I_3 = detB \tag{A.4}$$

If a material is hyperelastic, the following condition occurs: [57]

$$J = detF = \lambda_1\lambda_2\lambda_3 = 1 \qquad I_3 = 1 \tag{A.5}$$

where λ_1, λ_2 and λ_3 are the stretches in the main directions.

The principal invariants can be defined as:

$$I_1 = \lambda_1^2 + \lambda_2^2 + \lambda_3^2 \qquad I_2 = \lambda_1^2\lambda_2^2 + \lambda_1^2\lambda_3^2 + \lambda_2^2\lambda_3^2 \qquad I_3 = \lambda_1^2\lambda_2^2\lambda_3^2 \tag{A.6}$$

The main feature of the hyperelastic material is the deformation energy function W, which is a function of the deformation state: [57]

$$W = W(F) = \sum_{p=1}^{N} \frac{\mu_p}{\alpha_p}(\lambda_1^2 + \lambda_2^2 + \lambda_3^2 - 3) \tag{A.7}$$

where N indicates the number of terms in the strain energy function, μ_p are the constant shear moduli and α_p are a dimensionless constants.

The relationship between strain energy and deformation gradient allows to derive the stress response of the hyperelastic material known as Cauchy stress σ:[57]

$$\sigma_i = \lambda_i \frac{\partial W}{\partial \lambda_i} \tag{A.8}$$

In the incompressible Mooney-Rivlin material N=2, α_1=2, α_2=-2 and since the equation (A.5) is verified, the strain energy is given by:[57]

$$W = c_1(\lambda_1^2 + \lambda_2^2 + \lambda_3^2 - 3) + c_2(\lambda_1^{-2} + \lambda_2^{-2} + \lambda_3^{-2} - 3) = c_1(I_1 - 3) + c_2(I_2 - 3) \tag{A.9}$$

with the material parameters $c_1 = \mu_1/2$ and $c_2 = -\mu_2/2$.

The Cauchy-stress for a incompressible Mooney-Rivlin material is given by:[57]

$$\sigma = -pI + 2c_1B - 2c_2B^{-1} \tag{A.10}$$

where $p = \frac{2}{3}(c_1I_1 - c_2I_2)$ is the pressure, B^{-1} is the inverse of the Cauchy-Green tensor B.

In the incompressible Neo-Hooken material N=1, α_1=2 and using the first invariant I_1, the strain energy is given by:[57]

$$W = c_1(\lambda_1^2 + \lambda_2^2 + \lambda_3^2 - 3) = c_1(I_1 - 3) \tag{A.11}$$

which involves a single material parameter $c_1 = \mu_1/2$.

The Cauchy-stress for an incompressible Neo-Hookean material that derives from the strain energy is given by:[57]

$$\sigma = -pI + 2c_1B \tag{A.12}$$

where p is an undetermined pressure and B the Cauchy-Green tensor.

Appendix B

United States Life Tables

Table B.1: Life table for the male and female population: United States, 2017

Age (years)	**Probability of dying (male)**	**Probability of dying (female)**
55-56	0.007803	0.004829
56-57	0.008445	0.005221
57-58	0.009116	0.005613
58-59	0.009838	0.006011
59-60	0.010619	0.006429
60-61	0.01147	0.00688
61-62	0.012361	0.007371
62-63	0.01326	0.007903
63-64	0.01414	0.008481
64-65	0.015019	0.009111
65-66	0.015942	0.009793
66-67	0.017026	0.010568
67-68	0.018189	0.011436
68-69	0.019483	0.012474
69-70	0.02099	0.013659
70-71	0.022448	0.014881
71-72	0.024631	0.016529
72-73	0.02657	0.01821
73-74	0.02904	0.020011
74-75	0.031539	0.021903
75-76	0.034644	0.024322
76-77	0.038148	0.026899
77-78	0.04225	0.029886
78-79	0.046522	0.033413
79-80	0.051401	0.037065

Age (years)	Probability of dying (male)	Probability of dying (female)
80-81	0.056783	0.041478
81-82	0.062514	0.04615
82-83	0.069452	0.051681
83-84	0.077622	0.058587
84-85	0.086155	0.065586
85-86	0.09545	0.072855
86-87	0.105788	0.081115
87-88	0.118527	0.091618
88-89	0.132437	0.103241
89-90	0.147541	0.116041
90-91	0.163839	0.130061

Bibliography

[1] Cerebral Aneurysms Fact Sheet [National Institute of Neurological Disorders and Stroke]. 2020. https://www.ninds.nih.gov/disorders/patient-caregiver-education/fact-sheets/cerebral-aneurysms-fact-sheet.

[2] Brain Aneurysms [MSD MANUAL Professional Version]. 3 Nov 2020. https://www.msdmanuals.com/professional/neurologic-disorders/stroke/brain-aneurysms.

[3] Charles Vega, Jeremiah V Kwoon, Sea D Lavine. "Intracranial Aneurysms: Current Evidence and Clinical Practice." Am Fam Physician (2002 Aug 15); 66(4):601-8.

[4] Circulation and the Central Nervous System [Anatomy & Physiology]. http://pressbooks-dev.oer.hawaii.edu/anatomyandphysiology/chapter/circulation-and-the-central-nervous-system/.

[5] Circle of Willis [Wikipedia]. 2021. https://en.wikipedia.org/wiki/Circle_of_Willis.

[6] Purves, Dale; George J. Augustine; David Fitzpatrick; William C. Hall; Anthony-Samuel LaMantia; James O. McNamara; Leonard E. White. "Neuroscience, Fourth Edition." Sinauer Associates, Inc (2008). $ISBN 978 - 0878936977$.

[7] Boorder, Michiel J.; Grond, Jeroen; Dongen, Alice J.; Klijn, Catharina J.M.; Jaap Kappelle, L.; Rijk, Peter P.; Hendrikse, Jeroen. "Spect measurements of regional cerebral perfusion and carbondioxide reactivity: Correlation with cerebral collaterals in internal carotid artery occlusive disease". Journal of Neurology (24 October 2006); 253 (10):1285–1291. https://doi.org/10.1007/s00415-006-0192-1.

[8] Brain Aneurysm [Radiology]. https://med.nyu.edu/radiology/about-us/subspecialties/neuro-interventional/our-services/brain-aneurysm.

[9] Surgical Treatment: Clipping [Brain Aneurysm Foundation]. https://bafound.org/treatment/surgical-treatment-clipping/.

[10] Aneurisma Cerebrale [SINCH-Società Italiana Neurochirurgia]. 2015. http://sinch.it/documenti/uploads/sinc-1557318227_aanssinchaneurismicerebrali.pdf.

[11] Andrew White, Nicolas K Khattar, Nicolas K Khattar, Zaid Aljuboori, Jeffrey C. Obiora, Robert F. James. "Basic Endovascular Techniques: Direct, Balloon-Assisted, and Stent-Assisted Coil Embolization." Intracranial Aneurysms (2018); Edition:1; Chapter:21; Publisher:Elsevier. https://doi.org/10.1016/B978-0-12-811740-8.00023-X.

[12] Jeremie Dequidt, Maud Marchal, Christian Duriez, Erwan Kerien, Stephane Cotin. "Interactive Simulation of Embolization Coils: Modeling and Experimental Validation." Proceedings of the 11th international conference on Medical Image Computing and Computer-Assisted Intervention (February 2008).

[13] Christopher R.Durst M.D., Robert M.Starke M.D., M.Sc., John R. Gaughen Jr. M.D., Scott Geraghty M.D., K. Derek Kreitel M.D., Ricky Medel M.D., Nicholas Demartini M.D., Kenneth C. Liu M.D., Mary E. Jensen M.D., Avery J. Evans M.D. "Single-center experience with a dual microcatheter technique for the endovascular treatment of wide-necked aneurysms." American Journal of Neurosurgery (Nov 2014).

[14] L. Pierot, C. Cognard, L. Spelle and J. Moret. "Safety and Efficacy of Balloon Remodeling Technique during Endovascular Treatment of Intracranial Aneurysms: Critical Review of the Literature." American Journal of Neuroradiology (January 2012).

[15] Jun Kyeung Ko, M.D., Ph.D., Won Ho Cho, M.D., Ph.D., Seung Heon Cha, M.D., Ph.D., Chang Hwa Choi, M.D., Ph.D., Sang Weon Lee, M.D., Ph.D., Tae Hong Lee, M.D., Ph.D. "Semi-Jailing Technique Using a Neuroform3 Stent for Coiling of Wide-Necked Intracranial Aneurysms." Journal of Korean Neurosurgical Society (2017 Mar 1).

[16] K. Irie, M. Negoro, M. Hayakawa, J. Eayashi, and T. Kanno. "Stent Assisted Coil Embolization: the Treatment of Wide-necked, Dissecting, and Fusiform Aneurysms." Interventional Neuroradiology (2004 Oct 22).

[17] Elizabeth Hai Yen Du, Jai Jai Shiva Shankar. "LVIS Jr 'shelf' technique: an alternative to Y stent-assisted aneurysm coiling." Journal of Neurointerventional surgery (February 2016).

[18] Mascitelli JR, Moyle H, Oermann EK et-al. "An update to the Raymond-Roy Occlusion Classification of intracranial aneurysms treated with coil embolization." Journal of Neurointerventional Surgery (2015 July). https://doi.org/10.1136/neurintsurg-2014-011258.

[19] Soichiro Fujimura, Hiroyuki Takao, Takashi Suzuki, Chihebeddine Dahmani,Toshihiro Ishibashi, Hiroya Mamori, Makoto Yamamoto, Yuichi Murayama. "Hemodynamics and coil distribution with changing coil stiffness and length in intracranial aneurysms." Basic Science (19 December 2017).

[20] Soichiro Fujimura; Hiroyuki Takao; Takashi Suzuki; Chihebeddine Dahmani; Hiroya Mamori; Naoya Fukushima; Makoto Yamamoto and Yuichi Murayama. "Effect of Catheter Positions on Hemodynamics and Coil Formation after Coil Embolization." 2017 39th Annual International Conference of the IEEE Engineering in Medicine and Biology Society (EMBC). 2017.

[21] 510(k) Premarket Notification [FDA]. June 12, 2015. https://www.accessdata.fda.gov/scripts/cdrh/cfdocs/cfpmn/pmn.cfm?ID=K171747.

[22] ROBERT D. ECKER, MD, AND LEE R. GUTERMAN, MD, PHD. "Update on Currently Available Bioactive Coils." Neurovascular Intervention (JULY 2005).

[23] J.V. Byrne, G. Guglielmi. "Endovascular Treatment of Intracranial Aneurysms." Springer (1998).

[24] P.N. Sawyer, J.W. Pate, C.S. Weldon. "Relationship of abnormal and injury electric potential differences to intravascular thrombosis." Am J Physiol (1953); 175(1):108–112. https://doi.org/10.1152/ajplegacy.1953.175.1.108.

[25] Cerebral Coils [Endovascular Today]. https://evtoday.com.

[26] L.Pradelli, A.Wertheimer. "Pharmacoeconomics. Principles and Practice." SEEd (December 2012).

[27] Arias E. "United States Life Tables, 2017." National Vital Statistics Reports (June 24, 2019).

[28] S.HALLAN, A.ASBERG, B.INDREDAVIK & T.E.WIDEROE. "Quality of life after cerebrovascular stroke: a systematic study of patients' preferences for different functional outcomes." Journal of Internal Medicine (1999).

[29] Karoliina Aarnio, MD; Elena Haapaniemi, MD, PhD; Susanna Melkas, MD, PhD, Markku Kaste, MD, PhD; Turgut Tatlisumak, MD, PhD; Jukka Putaala, MD, PhD. "Long-Term Mortality after First-Ever and Recurrent Stroke in Young Adults." Department of Neurology, Helsinki University Central Hospital, Helsinki, Finland. Stroke (24 Jul 2014).

[30] Slot KB, Berge E, Sandercock P, et al. "Causes of death by level of dependency at 6 months after ischemic stroke in 3 large cohorts." Stroke (2009); 40(5):1585–1589.

[31] Chaisinanunkul N, Adeoye O, Lewis RJ, et al. "Adopting a patient-centered approach to primary outcome analysis of acute stroke trials using a utility-weighted modified Rankin scale." Stroke (2015); 46(8):2238–2243.

[32] Helical [Microvention]. https://www.microvention.com.

[33] Micrusframe S [J&J Medical Devices]. https://www.jnjmedicaldevices.com.

[34] R. Padolecchia, Guido Guglielmi, M. Puglioli, M. Castagna, Vincenzo Nardini, P.L. Collavoli, Giulio Guidetti, M. Dazzi, V. Zucchi, P. Narducci. "Role of electrothrombosis in aneurysm treatment with guglielmi detachable coils: An in vitro scanning electron microscopic study." American Journal of Neuroradiology (November 2001); 22(9):1757-60.

[35] ABC di farmacoeconomia [Pharmastar]. http://www.pharmastar.it/apple//binary_files/quaderni/ABC_Farmacoeconomia_53122.pdf

[36] Modified Rankin Scale for Neurologic Disability [MDCalc]. 2015. https://www.mdcalc.com.

[37] Bernard R Bendok, Rudy J Rahme, Complex Registry Group. "Complex shaped detachable platinum coil system for the treatment of cerebral aneurysms: The Codman Trufill DCS and Trufill DCS Orbit Detachable Coil System Complex Registry final results." J NeuroIntervent Surg (2013); 5(1):54-61.

[38] Joshua A Hirsch, Bernard R Bendok, Richard D Paulsen, Christophe Cognard, Jorge Campos, Mats Cronqvist. "Midterm Clinical Experience with a Complex shaped Detachable Platinum Coil System for the Treatment of Cerebral Aneurysms: Trufill DCS Orbit Detachable Coil System Registry Interim Results." J Vasc Interv Radiol (2007); 18(12):1487-94.

[39] Niemann et al. "Anatomically Conformable, Three-Dimensional, Detachable Platinum Microcoil System for the Treatment of Intracranial Aneurysms." AJNR Am J Neuroradiol (May 2004); 25:813–818.

[40] Ajay Malhotra, Xiao Wu, Waleed Brinjikji, Timothy Miller, Charles C Matouk, Pina Sanelli, Dheeraj Gandhi. "Pipeline Endovascular Device vs Stent-Assisted Coiling in Small Unruptured Aneurysms: A Cost-Effectiveness Analysis." Neurosurgery (2019).

[41] Megan E Barra, Karen Berger, Eljim P Tesoro, Gretchen M Brophy. "Periprocedural Neuroendovascular Antiplatelet Strategies for Thrombosis Prevention in Clopidogrel-Hyporesponsive Patients." Pharmacotherapy (2019 Mar).

[42] Jennifer A Frontera, Joseph Moatti, Kenneth M de los Reyes, Stephen McCullough, Henry Moyle, Joshua B Bederson, Aman Patel. "Safety and cost of stent-assisted coiling of unruptured intracranial aneurysms compared to coiling or clipping." J Neurointerv Surg (2014 Jan). https://doi.org/10.1136/neurintsurg-2012-010544.

[43] S.Iannazzo. "I modelli economico-sanitari: aspetti pratici e gestione dell'incertezza." SEEd (2006).

[44] Milton C Weinstein, Bernie O'Brien, John Hornberger, Joseph Jackson, Magnus Johannesson, Chris McCabe, Bryan R Luce, ISPOR Task Force on Good Research Practices-Modeling Studies. "Principles of good practice for decision analytic modeling in health-care evaluation: report of the ISPOR Task Force on Good Research Practices-Modeling Studies." Value in Health (2003). https://doi.org/10.1046/j.1524-4733.2003.00234.x.

[45] Types of aneurysm. https://previews.123rf.com/images/maniki81/maniki812003/maniki81200300017/143480381-types-of-aneurysm-fusiform-pseudoaneurysm-saccular-\\dissecting-ruptured-simple-medical-anatomy-illust.jpg.

[46] Miguel O. Bernabeu, Rupert W. Nash, Derek Groen, Hywel B. Carver, James Hetherington, Timm Krüger and Peter V. Coveney, "Impact of blood rheology on wall shear stress in a model of the middle cerebral artery." Royal Society (6 April 2013). https://doi.org/10.1098/rsfs.2012.0094.

[47] Hemorheology [Wikipedia]. https://en.wikipedia.org/wiki/Hemorheology.

[48] Boyd J, Buick JM, Green S. "Analysis of the Casson and Carreau–Yasuda non-Newtonian blood models in steady and oscillatory flows using the lattice Boltzmann method." Phys. Fluids 19, 093103 (2007). https://doi.org/10.1063/1.2772250.

[49] F. Yilmaz and M. Y. Gundogdu. "A Critical Review on Blood Flow in Large Arteries; Relevance to Blood Rheology, Viscosity Models, and Physiologic Conditions." Korea-Australia Rheology Journal (2008).

[50] Aneurysms [Medbullets]. Moises Dominguez (2020). https://step1.medbullets.com/neurology/113020/aneurysms.

[51] Bo Liu, Qi Li, Jisheng Wang, Hu Xiang, Hong Ge, Hui Wang, Peng Xie. "A Highly Similar Mathematical Model for Cerebral Blood Flow Velocity in Geriatric Patients with Suspected Cerebrovascular Disease." Scientific Reports (2015).

[52] R. Torii, M. Oshima, T. Kobayashi, K. Takagi, and T.E. Tezduyar, "Influence of wall elasticity in patient-specific hemodynamic simulations", Computers & Fluids (January 2007).

[53] Torii, R., Oshima, M., Kobayashi, T., Takagi, K., Tezduyar, T.E., 2010. "Influence of wall thickness on fluid–structure interaction computations of cerebral aneurysms." International Journal for Numerical Methods in Biomedical Engineering (March 2007).

[54] Abruzzo, T., Shengelaia, G., Dawson, R., Owens, D., Cawley, C., Gravanis, M. "Histologic and morphologic comparison of experimental aneurysms with human intracranial aneurysms." Am. J. Neuroradiol (1998) 19:1309–1314.

[55] Artery [Wikipedia]. https://en.wikipedia.org/wiki/Artery.

[56] Von Mises yield criterion [Wikipedia]. https://en.wikipedia.org/wiki/Von_Mises_yield_criterion.

[57] B.K. Toth, G. Raffai, and I. Bojtar. "Analysis of the mechanical parameters of human brain aneurysms." Acta of Bioengineering and Biomechanics (2005).

[58] COMSOL Multiphysics, version 5.3, Structural Mechanics Module User's Guide 2008.

[59] COMSOL Multiphysics, version 3.4, User's Manual 2008.

[60] Amir Shamloo, Milad Azimi Nejad, Milad Saeedi. "Fluid–structure interaction simulation of a cerebral aneurysm: Effects of endovascular coiling treatment and aneurysm wall thickening." Journal of the Mechanical Behavior of Biomedical Materials (2017).

[61] Castro, M., Putman, C., Cebral, J. "Computational fluid dynamics modeling of intracranial aneurysms: effects of parent artery segmentation on intra-aneurysmal hemodynamics." American Journal of Neuroradiology (September 2006); 27 (8) 1703-1709.

[62] Xiang, J., Tremmel, M., Kolega, J., Levy, E.I., Natarajan, S.K., Meng, H. "Newtonian viscosity model could overestimate wall shear stress in intracranial aneurysm domes and underestimate rupture risk." J Neurointerv Surg (2011 Sep).

[63] Hoi, Y., Woodward, S.H., Kim, M., Taulbee, D.B., Meng, H. "Validation of CFD simulations of cerebral aneurysms with implication of geometric variations." J.Biomech. Eng (2006); 128, 844–851.

[64] Lu, G., Huang, L., Zhang, X., Wang, S., Hong, Y., Hu, Z., et al. "Influence of hemodynamic factors on rupture of intracranial aneurysms: patient-specific 3D mirror aneurysms model computational fluid dynamics simulation." Am. J.Neuroradiol (2011); 32, 1255–1261.

[65] Isaksen, J.G., Bazilevs, Y., Kvamsdal, T., Zhang, Y., Kaspersen, J.H., Waterloo, K., et al. "Determination of wall tension in cerebral artery aneurysms by numerical simulation." Stroke (2008); 39, 3172–3178.

[66] MacDonald, D.J., Finlay, H.M., Canham, P.B. "Directional wall strength in saccular brain aneurysms from polarized light microscopy." Annals of Biomedical Engineering (2000); 28, 533–542.

[67] Seyed Esmail Razavi, Vahid Farhangmehr, Nafiseh Zendeali. "Numerical investigation of the blood flow through the middle cerebral artery." BioImpacts (2018); 8(3), 195-200.

[68] Alvaro Valencia, Patricio Burdiles, Miguel Ignat, Jorge Mura, Eduardo Bravo, Rodrigo Rivera, and Juan Sordo. "Fluid Structural Analysis of Human Cerebral Aneurysm Using Their Own Wall Mechanical Properties." Computational and Mathematical Methods in Medicine (2013).

[69] Guide to the methods of technology appraisal 2013 [NICE]. 2013. https://www.nice.org.uk/process/pmg9/resources/guide-to-the-methods-of-technology-appraisal-2013-pdf-\\2007975843781.

[70] Nohra el-Chalouhi, Pascal M. Jabbour, Stavropoula I. Tjoumakaris, Robert M. Starke, Aaron S. Dumont, Haisong Liu, Robert Rosenwasser, Sedeek El Moursi, L. Fernando Gonzalez. "Treatment of Large and Giant Intracranial Aneurysms: Cost Comparison of Flow Diversion and Traditional Embolization Strategies." Journal World Neurosurgery (2014).

[71] Dmitry Dukhovny, John A.F. Zupancic. "Economic Evaluation With Clinical Trials in Neonatology." NeoReviews (February 2011). https://doi.org/10.1542/neo.12-2-e69.

[72] Hetts SW, Turk A, English JD, et al. "Stent-assisted coiling versus coiling alone in unruptured intracranial aneurysms in the matrix and platinum science trial: safety, efficacy, and mid-term outcomes." American Journal of Neuroradiology (2014); 35(4):698-705.

[73] Nishido H, Piotin M, Bartolini B, Pistocchi S, Redjem H, Blanc R. "Analysis of complications and recurrences of aneurysm coiling with special emphasis on the stent-assisted technique." American Journal of Neuroradiology (2014); 35(2):339-344.

[74] M Haithem Babiker, Brian Chong, L Fernando Gonzalez, Sachmanik Cheema, David H Frakes. "Finite element modeling of embolic coil deployment: multifactor characterization of treatment effects on cerebral aneurysm hemodynamics." J Biomech (2013); 46:2809–16. https://doi.org/10.1016/j.jbiomech.2013.08.021.

[75] Soichiro Fujimura, Hiroyuki Takao, Takashi Suzuki, Chihebeddine Dahmani, Hiroya Mamori, Makoto Yamamoto, Yuichi Murayama. "Hemodynamic effects from coil distribution with realistic coil models in an aneurysm." 2016 38th Annual International Conference of the IEEE Engineering in Medicine and Biology Society (EMBC) (2016 Aug). https://doi.org/10.1109/embc.2016.7591433.

[76] Michel Piotin, Laurent Spelle, Charbel Mounayer, Marco T Salles-Rezende, Daniel Giansante-Abud, Ricardo Vanzin-Santos, Jacques Moret. "Intracranial aneurysms: treatment with bare platinum coils-aneurysm packing, complex coils, and angiographic recurrence." Radiology (May 2007). https://doi.org/10.1148/radiol.2431060006.

[77] Takao H, Ishibashi T, Saguchi T, et al. "Validation and initial application of a semiautomatic aneurysm measurement software: a tool for assessing volumetric packing attenuation." American Journal of Neuroradiology (April 2014); 35:721–6.